DISTRIBUTION OF VOLATILES IN THE GLASSY RIMS OF SUBMARINE PILLOW BASALTS

by

John Rutledge Delaney

A Dissertation Submitted to the Faculty of the

DEPARTMENT OF GEOSCIENCES

In Partial Fulfillment of the Requirements
For the Degree of

DOCTOR OF PHILOSOPHY

In the Graduate College

THE UNIVERSITY OF ARIZONA

1 9 7 7

THE UNIVERSITY OF ARIZONA

GRADUATE COLLEGE

I hereby recommend that this dissertation prepared under my direction by JOHN RUTLEDGE DELANEY

entitled DISTRIBUTION OF VOLATILES IN THE GLASSY RIMS OF SUBMARINE PILLOW BASALTS

be accepted as fulfilling the dissertation requirement for the degree of Doctor of Philosophy

J. Dauguly — 4/26/77

Dissertation Director — Date

As members of the Final Examination Committee, we certify that we have read this dissertation and agree that it may be presented for final defense.

	Apr. 26 1977
Michael J. Drake	April 26, 1977
	26 Apr 77
	May 2, 1977
	May 13, 1977

Final approval and acceptance of this dissertation is contingent on the candidate's adequate performance and defense thereof at the final oral examination.

STATEMENT BY AUTHOR

This dissertation has been submitted in partial fulfillment of requirements for an advanced degree at The University of Arizona and is deposited in the University Library to be made available to borrowers under rules of the Library.

Brief quotations from this dissertation are allowable without special permission, provided that accurate acknowledgment of source is made. Requests for permission for extended quotation from or reproduction of this manuscript in whole or in part may be granted by the head of the major department or the Dean of the Graduate College when in his judgment the proposed use of the material is in the interests of scholarship. In all other instances, however, permission must be obtained from the author.

SIGNED: 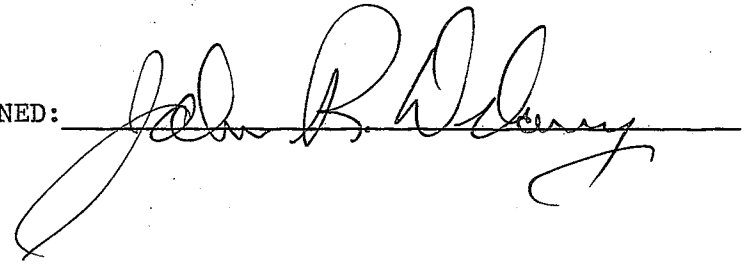

ACKNOWLEDGMENTS

My initial interest in magmatic gases was sparked by interaction with B. E. Nordlie and kept alive through discussions with T. M. Gerlach and W. E. Colony. Without the collaboration of D. W. Muenow, Department of Chemistry, University of Hawaii, this study would not have been possible. I deeply appreciate the excellent and enthusiastic advising and the financial assistance I have received from Jibamitra Ganguly, whose input to this dissertation has fundamentally improved the final product. Stimulating and critical discussions with, as well as periodic monetary injections from. T. P. Loomis particularly, P. E. Damon and M. J. Drake, are gratefully acknowledged. A. Meijer has provided challenging criticism and valuable samples from the Marianas Interarc Basin, both of which have helped to place the major conclusions of this work on firmer ground. E. A. Mathez, Department of Geological Sciences, University of Washington, generously provided ideas, time, critical follow-up samples, and microprobe analyses without which my dissertation would have been much less complete. R. B. Scott, of Texas A & M University, made samples available from the Transatlantic Geotraverse, sponsored by the National Oceanic and Atmospheric Administration. Assistance with some of the initial gas analyses from E. K. Gibson at the Johnson Spacecraft Center in Houston, and C. S. Lewis and J. Cripe, of Arizona State University in Tempe, has contributed to the present results. E. J. McCullough's continuing moral and financial support were important ingredients in the successful

conclusion of this project. The editorial assistance, quiet confidence, and boundless patience of H. J. Delaney have touched every page of this dissertation.

TABLE OF CONTENTS

TABLE OF CONTENTS--Continued

LIST OF ILLUSTRATIONS

LIST OF TABLES

ABSTRACT

Glass-vapor inclusions within olivine and/or plagioclase phenocrysts quenched in the glassy rims of eight typical oceanic tholeiitic pillow basalts from the Mid-Atlantic Ridge (3), Kolbeinsey Ridge (1), Juan de Fuca Ridge (1), Paul Revere Ridge (1), the ocean floor near the Explorer Seamount (1), and Hawaiian East Rift (1), all contain less than 0.01 wt % H_2O, between 0.2 and 0.4 wt % CO_2 and about 0.08 to 0.15 wt % sulfur. The enclosing matrix glasses contain 0.1 to 0.35 wt % H_2O, 0.04 to 0.09 wt % CO_2, and about 0.1 to 0.15 wt % sulfur.

The two- to four-fold enrichment of CO_2 in the inclusions compared to the matrix glass can be explained either by crystal growth (inclusion formation) in a magma which was initially richer in CO_2, or by volatile concentration at the crystal magma interface during crystal growth. Neither crystal growth kinetics, nor pressure-induced diffusional gradients caused by decompression after inclusion entrapment, could have produced the severe depletion of water in the inclusions. The data seem to require the source regions for these basalts to be virtually depleted in water, and possibly richer in CO_2 than the magmas quenched on the ocean floor. Apparently, water enters the magma after inclusion formation and before quenching.

INTRODUCTION

Petrogenetic models for basalts depend critically upon the abundance and character of volatiles in the system (Holloway and Burnham, 1972; Eggler, 1974, 1975, 1976; Kushiro, 1972; Mysen and Boettcher, 1975a, 1975b). Water and, to a lesser extent carbon dioxide, exert freezing point depression effects upon mantle mineral assemblages at pressures to 30 kb. Hydrous and carbonate phases must have a substantial influence upon minor and trace-element fractionation between melt and crystalline residuum. Both factors indicate a need to understand relative and absolute volatile abundances in source regions for major magma types including oceanic basalts. In addition, determination of the rate and mechanism of volatile flux from such sources to the surface environment is an important step toward establishing realistic models of the earth's volatile budget. Mantle-derived gases emplaced in the surface environment by volcanic activity in the open-ocean basins probably represent a major fraction of the current volatile contribution from the mantle because of the abundance of oceanic basalts, and because a significant portion of island arc volcanic volatiles apparently have a recycled nature.

Glassy Rims of Pillow Basalts

Over the past decade, Moore and his co-workers (Moore, 1965, 1970; Moore and Calk, 1971; Moore and Fabbi, 1971; Moore and Schilling, 1973) have largely been responsible for establishing the petrologic significance of glassy rims on submarine pillow basalts. In contrast to

subaerial eruptions, basalts emplaced on the ocean floor are rapidly quenched under confining pressures which are determined by the depth of eruption beneath the ocean (100 m ∿ 10 bars). Although volatile solubility in silicate melts depends on pressure, temperature, and bulk composition, the solubility limits for water and carbon dioxide in oceanic basalts are primarily a function of pressure (Hamilton, Burnham, and Osborn, 1964; Eggler, 1974, 1975, 1976; Mysen, Eggler, Seitz, and Holloway, 1976; Mysen, 1976; Khitarov and Kadik, 1973), because pressure is the major variable for such magmas from source region to ocean floor. The outer centimeter of pillow basalts is probably quenched in less than ten seconds (Moore, 1975) and represents one of the most volatile-rich natural samples of basaltic magma currently available for laboratory study.

Pillow rims are apparently more representative of the pre-eruption magma than the more slowly cooled, partly crystalline, pillow interiors, which commonly react with seawater. For instance, Dymond and Hogan (1973) conclude that the noble gas composition of crystalline pillow interiors has developed by exchange with seawater; the pillow rims, in contrast, display a distinctly different noble gas abundance pattern. Glassy rims of pillow basalts also exhibit $^{3}He/^{4}He$ ratios which are about 10 times the atmospheric value (Lupton and Craig, 1976a,b). Craig and Lupton (1976, p. 408) have shown that the average δD for ^{3}He-rich glasses from the East Pacific Rise is between -60 and -80‰ relative to Standard Mean Ocean Water (SMOW), representing, according to them, "the first clearcut measurements of water from the mantle." Similar values

were obtained by Friedman cited in Moore (1970) for glassy pillow rims from Hawaii. Thus, examination of unaltered pillow basalt rims from mid-ocean ridges may be expected to provide significant insight into volatile abundance patterns of the basalts in or near their source regions. Such an approach has been taken by Moore (1965, 1970), Moore and Fabbi (1971), and Moore and Schilling (1973) to estimate the "juvenile" sulfur (800 $\pm$ 150 ppm) and water (0.2-0.4 wt%) content of K-poor oceanic tholeiites.

There is, however, at least one potentially important limitation to such an approach. All glassy pillow basalt rims, even those from as deep as 5000 m (Moore, 1965), are reported to contain vesicles which are on the average 1% by volume and less than 1 mm in diameter. These vesicles permit the interpretation that the magma has been degassed to an unknown extent prior to eruption and quenching on the ocean floor. To estimate absolute abundances, or ratios, of volatiles dissolved in the magma at greater depths, one must contend with an unknown amount of prior degassing. In view of this problem, attention was focused in this study on the volatile content of the glass-vapor inclusions trapped within the phenocrysts quenched in the glassy rims. It was expected that these inclusions had sampled magma during an earlier stage of development, perhaps before the magma had undergone significant degassing. Contrasting the volatile content of the inclusions with that of the enclosing, quenched matrix glass constitutes the principal contribution of this work.

Current Concepts of Basaltic Magmatic Gases

In view of the nature and objective of the present work, it seems appropriate to provide a brief summary of current concepts of basaltic magmatic gases (for more extensive review see Anderson, 1975). Principal approaches to the investigation of basaltic gases have been:

1) Collection and analysis of gases erupted from active basaltic volcanos (Jaggar, 1940; Iwasaki, Ozawa, Yoshida, Katsura, Iwasaki, and Kamada, 1963; Naughton, Heald, and Barnes, 1963; Naughton, Derby, and Glover, 1969; Finlayson, Barnes, and Naughton, 1968; Nordlie, 1971; Sigvaldason and Elisson, 1968; Tazieff, Leguern, Carbonnelle, and Zettwoog, 1972; Tazieff, 1966; Swanson and Fabbi, 1973; Leguern, 1972).
2) Analysis of gases contained in volcanic rocks (Chamberlain, 1908; Shepherd, 1938; Roedder, 1965; Anderson, 1974; Moore, 1965, 1970; Moore and Schilling, 1973; Moore and Fabbi, 1971; Swanson and Fabbi, 1973).

These workers conclude that basaltic gas compositions fall principally within the system C-O-S-H. Argon, nitrogen, bromine, chlorine, and fluorine are minor components, and H_2S, H_2, and CO are minor species under most near-surface magmatic conditions (Gerlach and Nordlie, 1975).

There are, however, serious problems and disagreements about characterization of magmatic gases in the near-surface environment. For example, Puccetti and Buddemeier (1974) observe that there is currently inadequate or conflicting data to account for the large amounts of CO_2

evolving from Kilauea in terms of CO_2-solubility and abundance of erupted magma. Anderson (1975) admits that CO_2 is poorly understood as a magmatic gas. Nordlie (1971) proposes a generalized basaltic gas composition of approximately equal molar amounts of CO_2, H_2O, and SO_2. But Anderson (1975) concluded that there is no single magmatic gas phase. He further states (p. 37) "volcanic gas emitted at surface pressure is generally very rich in H_2O because H_2O is the principal gas dissolved in most melts." Naughton and colleagues (Naughton, Heald, and Barnes, 1963; Heald, Naughton, and Barnes, 1963; Naughton, Derby, and Glover, 1969) apparently agree with Anderson, as they have consistently held that Hawaiian volcanic gases are H_2O-rich. Moore (1965) pointed out that even though pillow basalts as deep as 5000 m near Hawaii were vesiculated, they were drastically undersaturated with respect to water at the pressure corresponding to that depth. Anderson (1975) agrees with Moore and points out that CO_2 is also distinctly undersaturated in quenched rims of pillow basalts; he comments that the explanation of the vesicles is not obvious. Drawing upon data from Moore (1965), Moore and Calk (1971), and Anderson and Wright (1972), Anderson (1975) estimates the equilibrium composition of gas which would exist in vesicles within the Hawaiian pillow basalts by assuming sulfur gases (SO_2) make up the difference between total pressure and his (Anderson's) solubility-based estimates of CO_2 and H_2O partial pressures. He concludes that at about 470 bars and 1200°C the gas would be 60% SO_2, 20% H_2O, 10% CO_2, and 10% H_2S. He then points out that the same lavas, if erupted at the surface, would produce a gas which was 86% H_2O, 1.4% CO_2, 11.5%

SO_2 and very little else. Sigvaldason and Elisson (1968) sampled gases from Surtsey which were 86% H_2O, 4.7% H_2, 5.7% CO_2, and 2.7% SO_2. Arnason and Sigurgeirsson (1968) determined δD SMOW values of about -55% for water condensed from hot fumaroles at Surtsey, which compares well with previously cited deuterium contents of glassy pillow rims (Craig and Lupton, 1976; Moore, 1970).

Mathez (1976) has recently shown a positive linear correlation between sulfur and iron content of seafloor basalt glasses. Further, each of the 34 pillow basalt rims he examined contained spherical sulfide grains. These were interpreted by him to be immiscible under magmatic conditions. He concluded that sulfur solubility in seafloor basalts is dominantly controlled by the iron content of the magma. This conclusion is consistent with the experimental work of Haughton, Roeder, and Skinner (1974) and Katsura and Nagashima (1974). Moore and Fabbi (1971) and Moore and Schilling (1973) have shown that the sulfur content of seafloor basalts does not vary significantly as a function of depth beneath the ocean until vesiculation becomes an important process. At depths shallower than this the sulfur content (800-1400 ppm) becomes systematically reduced, with continued degassing, to normal subaerial concentrations of about 200 ppm.

Differing initial abundances, solubilities, degrees of partial melting, fractional crystallization, and contamination before and during eruptions severely complicate attempts to generalize basaltic magmatic gas compositions. In addition, problems inherent with <u>in situ</u> gas collections during volcanic eruptions include varying degrees of personal

danger, unpredictable and poorly planned eruption events, groundwater and atmospheric contamination, and the almost insurmountable problem of accurately correlating specific masses of erupted gas to known masses of magma. Volcanic gas collections can provide, at best, qualitative information about gas abundances originally dissolved in erupting magma. They may be severely misleading when generalized to the magma source.

In contrast, practical and scientific advantages of studying fresh basaltic glasses quenched on the ocean floor are:

1) Safe, unhurried, albeit expensive, sample collection through drilling and dredging;
2) Readily removable contamination in the form of alteration products;
3) Well-controlled, replicate analyses of equal-quality samples; and most important;
4) The opportunity to establish volatile-to-magma mass ratios.

Yet, some difficulties persist, such as the effects of varying degrees of partial melting, fractional crystallization, and pre-eruption contamination. However, these problems should become somewhat more tractable when comparisons can be made between accurately determined volatile mass abundances and indices of differentiation. That is, it may be possible to evaluate the premise that less-differentiated samples contain more "primitive" volatiles in terms of gases lost and/or contamination accumulated.

SAMPLE DESCRIPTION AND ANALYSIS

This study was initiated with pillow basalts dredged from the interior rift valley of the Mid-Atlantic Ridge (MAR) between 25 and 30° north latitude. Additional porphyritic glassy submarine basalts dredged from Kolbeinsey Ridge (north of Iceland), Juan de Fuca and Paul Revere Ridges, the ocean floor near the Explorer Seamount, the east rift of Hawaii, and the Marianas Interarc Basin were added to pursue initial findings. It is convenient to refer to ridge and island basalts as "open-ocean basin" basalts, in contrast to basalts from a back-arc or interarc environment. Data on sample numbers, latitude, longitude, oceanographic features, dredge depth, near liquidus phases, and major-element analyses are included in Table I. Most of the samples were dredged from depths between about 2000 and 4000 m below sea level. These depths are assumed to correspond to the eruption and quenching depths of the original lava.

The glassy rinds of the pillow lavas from most of these samples are typical low K tholeiitic basalts consistent with the minor-element criteria of Pearce, Gorman and Birkett (1975) for oceanic basalts (Figure 1). The glasses are olivine-normative tholeiites which are close to silica saturation and most contain plagioclase and/or olivine crystals with or without minor spinel.

All samples studied have spherical vesicles quenched in the glassy portions of the pillow basalt rims which are very similar to those described by Moore (1965, 1970), Moore and Calk (1971), Moore and

Table I. Summary of Sample Number, Longitude-latitude, Associated Feature, Dredge Depth, Chemical Analyses, and near Liquidus Phases for Glassy Rims of Open-ocean Pillow Basalts.

	T4-73R307-2A1[a] 26°09.66'N 44°47.4'W MAR[b]	T4-73R308-3A3 26°07.3'N 44°48.8'W MAR	T4-73R308-4C1 26°18.2'N 44°42.1'W MAR	T4-73R311-6A4 26°02.3'N 44°36.8'W MAR	T3-72D249-7A4 25°18.2'N 45°36.8'W MAR	T3-71D159-10C1 29°47'N 43°44'W MAR	T3-71D159-10C4 29°47'N 43°44'W MAR	T3-71D159 10C18 29°47'N 43°44'W MAR	Tr-139-25D (R1-24)[c] 69°09'N 16°13'W KR[g]	EN-70-25-6-70 (R1-3) 50°00'N 129°27'W PRR[h]	TTO29-011-2 (R1-8) 46°21.8'N 129°58.4'W JFR[i]	TTO63-072-30 (R1-18-2) 48°57.2'N 130°49.2'W ES[j]
Depth (M)	3148	3083	4136	3100	3618	2743-1920	2743-1920	2743-1920	1100-1200	1400-1700	2400-2600	2300-2500
SiO_2	49.90	49.68	49.10	50.50	51.00	47.60	47.50	49.50	51.18	48.79	48.02	48.52
TiO_2	1.44	1.54	1.80	1.60	1.54	.98	.96	1.70	.81	1.14	1.16	1.58
Al_2O_3	16.05	16.50	16.45	15.00	15.05	16.66	16.70	15.30	14.69	16.77	17.08	16.78
Fe_2O_3[d]	.68	.82	1.20	1.09	1.01	.38	.58	1.14	---	---	---	---
FeO	8.57	8.95	9.25	9.33	8.95	9.20	9.05	10.25	9.41[d]	9.90[d]	9.77[d]	9.71[d]
MgO	8.70	7.30	7.55	8.10	7.95	10.40	10.60	8.35	8.53	8.67	9.28	8.60
CaO	10.90	11.40	10.90	10.60	10.70	10.90	11.06	10.40	13.31	11.43	11.63	11.43
Na_2O	2.80	2.94	3.15	2.98	2.88	2.73	2.60	2.95	1.78	2.65	2.61	3.04
K_2O	.10	.09	.09	.11	.10	.04	.05	.09	.06	.05	.03	.06
MnO	.17	.19	.17	.19	.18	.16	.18	.19	.19	.17	.18	.17
P_2O_5	.14	.14	.20	.06	.17	.07	.10	.16	.06	.08	.06	.13
Ni (ppm)	75	130	52	40	45	265	65	70	60	240	545	230
TOTAL	99.45	99.55	99.86	99.66	99.53	99.12	99.38	100.03	100.02	99.65	99.82	100.02
near liquidus phases	(Ol)[e]	(Ol)	Pc-15%[e] (Ol)	Ol	--	Pc-12%[e] Ol-16% (Sp)	Pc-13% Ol-14% (Sp)	(Ol)	Pc-20% (Ol)	Ol-3%	Ol-12% (Pc)	Ol-5%

[a]Underlined portion of sample designation is the number used as referenced in text. All analyses by atomic absorption (App. A) unless otherwise specified.
[b]Mid-Atlantic Ridge
[c]Electron microprobe analysis of glass (samples with Rl designation are from University of Washington Oceanography Department Sample Library).
[d]Total iron as FeO. Ferrous iron by wet chemical techniques (App. A).
[e]Phases which occur in glassy rind of pillow basalts surrounded by glass. Pc = plagioclase, Ol = olivine, Sp = chrome spinel, ( ) = a phase less than 2% by volume.
[f]P_2O_3 by electron microprobe
[g]Kolbeinsey Ridge
[h]Paul Revere Ridge
[i]Juan de Fuca Ridge
[j]Explorer Seamount

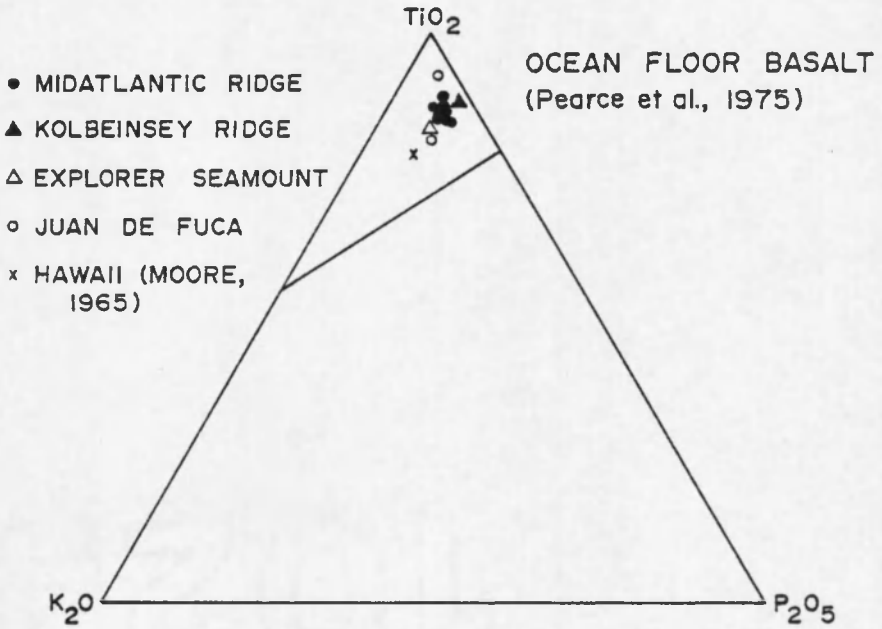

Figure 1. TiO_2-K_2O-P_2O_5 Triangular Plot from Pearce, Gorman, and Birkett (1975) Used to Identify Basalts from Oceanic Environments. -- The dividing line separates 93% of 222 ocean floor and ocean ridge basalts into the upper field.

Schilling (1973), Mathez and Yeats (1976). The vesicles occupy approximately 1 to 3 volume percent of the well-quenched glass near the outer portion of the glassy rim. They vary in size from less than 1 micron to as much as 2 mm diameter and are frequently lined with what appear to be sulfide spherules described by Moore and Calk (1971). Approximately 30% of the vesicles in the well-quenched portion of the glassy rim are attached to crystals and the rest appear to have resulted from homogeneous nucleation. The percentage of vesicles increases inward from the well-quenched outer rim as the total percentage of glass decreases and spherulitic quench crystals become more abundant.

Crystalline phases in the outer portions of the glassy rims probably represent near-liquidus phenocrysts (see discussion below). Plagioclase crystals in 4C1, 10C1, 10C4, and R1-24 range from .5 mm to 1 cm in diameter, are commonly elongate, anhedral and composite, and contain variable amounts of glass-vapor inclusions. Some plagioclases may have less than 0.5 volume percent inclusion while others contain more than 10 volume percent inclusions. Larger olivine crystals in all samples are anhedral, equant, and range up to 0.5 cm in diameter. Smaller olivine crystals (<100μm diameter) tend to be euhedral with well-developed crystal faces. The percentage of inclusions in olivine is usually less than in plagioclase and rarely exceeds 1 volume percent.

Mineral-Glass Equilibrium and Temperature Estimates

Analyses of crystalline phases from six of the MAR samples and the fresh glassy rims from most of the pillow basalts were determined by

electron probe microanalysis at the University of Washington Geological Sciences Department. All analyses were conducted with mineral standards having compositions similar to the unknowns, and data corrections were by the EMPADR VII reduction program (Rucklidge and Gasparrini, 1969). Mineral analyses were made with a 2-4μm diameter beam at 15 KEV acceleration potential and 80-100 anoamp sample current. Glass analyses involved similar conditions but a 15-20μm beam diameter was used. The combination of large beam diameter and moderate sample current in the glass analyses effectively eliminated alkali loss. Counting times were terminated on fixed beam current, and their durations (apx. 10-30 sec.) depended on the concentrations of elements being analyzed. Experience shows that with the exception of Ca, good mineral standards yield good glass analyses when formal reduction procedures are followed. These standards (elements for which they were used) were bytownite (Si,Al), synthetic Ti diopside (Ti), olivine (Fe,Mg), albite (Na), orthoclase (K), synthetic chalcopyrite (S), apatite (P), and garnet (Mn). Ca was calculated by a curve fit to other glass standards. By reproducing analyses of glass standards run with unknowns, accuracies are estimated relative to absolute element concentrations of <1.5% for Si, Ti, Al, and Na, and 1.5-2.5% for Ca, Fe, and Mg. The accuracy of the sulfur data was confirmed with additional sulfide standards. Each matrix glass analysis is an average of ten random spot analyses. The homogeneity index reported for one sample of matrix glass (Appendix B) is typical of others and demonstrates that glasses are generally homogeneous by this criterion. Inclusion glass also appeared homogeneous when it was possible to

analyze more than one spot. In several instances attempts were made to identify chemical gradients in glass adjacent to crystals and across inclusion glass, but none were found.

Inclusion-bearing Crystals: Phenocrysts or Xenocrysts?

The possibility that inclusion-bearing crystalline phases are xenocrysts dispersed through the magma from a source external to the system was raised by Roedder (1965). Disaggregation of noncognate xenoliths or nodules may introduce crystals whose volatile content is not related to the earlier history of the enclosing magma. To explore this possibility, electron microprobe data for coexisting plagioclase-glass and olivine-glass pairs from six of the MAR samples are plotted in Figure 2. Compositional relationships between glass-mineral pairs are summarized in terms of Mg/(Mg + Fe) or Ca/(Ca + Na) mole percent for crystals and for coexisting glasses. The horizontal axis of these particular diagrams is analogous to the compositional axis of a classic T-X diagram depicting the solid solution loops for the pure olivine and pure plagioclase systems. Analyses of phenocrysts and microcrysts (maximum dimension <50μm) are represented by squares and crosses, respectively. Data related to plagioclase-glass pairs are plotted above the line, and olivine-glass data from the same sample are plotted below the line. The circles and triangles represent mole percentage values of Ca/(Ca + Na) and Mg/(Mg + Fe), respectively, in the enclosing matrix glasses.

Individual olivine grains are compositionally homogeneous; olivine phenocrysts and microcrysts from a single sample cluster tightly

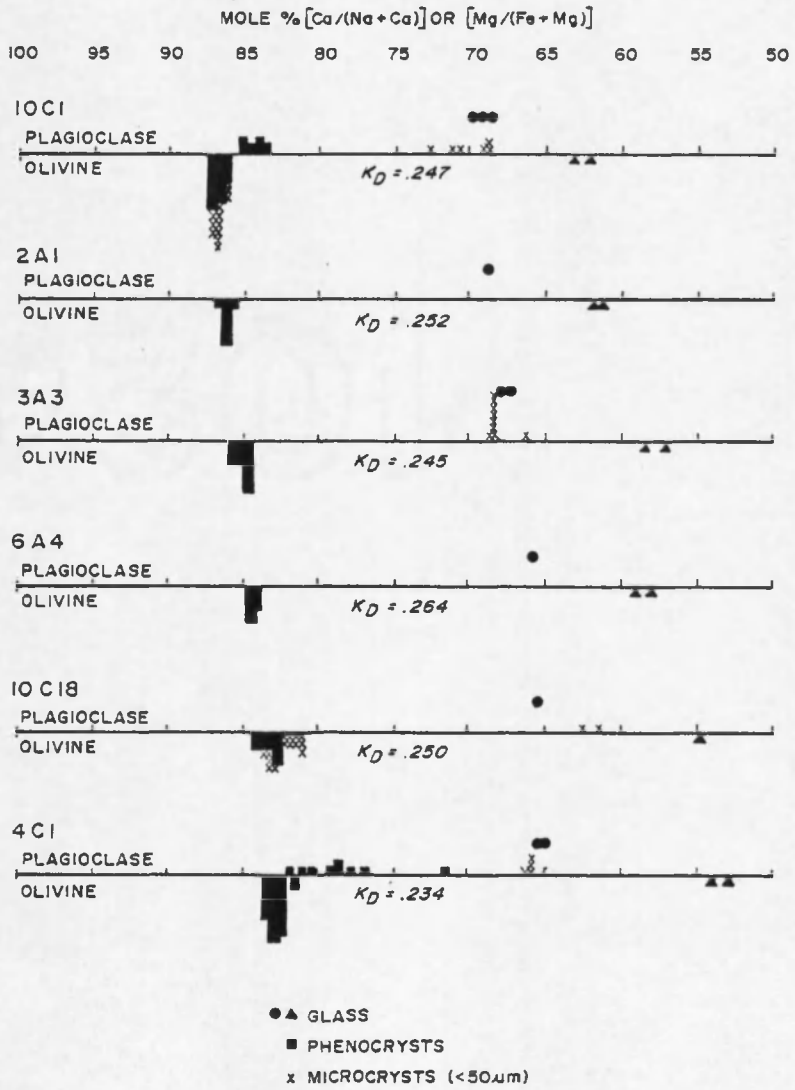

Figure 2. Microprobe Analyses of Minerals and Glass. -- Samples are from the rims of six basalts from the interior valley of the Mid-Atlantic Ridge. Horizontal axis is mole percent of either Ca/(Na + Ca) or Mg/(Fe + Mg). For the minerals this corresponds to the anorthite (plotted above the line) or forsterite (plotted below the line) component, respectively. For the glass it is proportional to the maximum anorthite or forsterite component dissolved in the melt. The value of K_D as defined by Roeder and Emslie (1970) is $(X_{FeO}/X_{MgO})^{ol}/(X_{FeO}/X_{MgO})^{magma}$. See text for discussion.

about an average value for that particular rock. The larger crystals are usually anhedral and subrounded while the microcrysts are commonly euhedral. The range of olivine compositions for all samples analyzed is Fo_{87} (sample 10C1) to Fo_{82} (sample 4C1). Mg/(Mg + Fe) in glass surrounding the crystals shows a trend sympathetic to iron enrichment in the crystals when the six samples are considered in sequence from 10C1 to 4C1. This trend is reflected in the consistency of the K_D values, defined by Roeder and Emslie (1970) as $K_D = (X_{FeO}/X_{MgO})^{ol}/(X_{FeO}/X_{MgO})^{magma}$. For the six samples, the values of K_D closely approximate 0.25, differing from K_D values for basaltic systems obtained experimentally by Roeder and Emslie (1970) which cluster about 0.30. They concluded that K_D is insensitive to temperature changes. Although their work was conducted at one atmosphere in the temperature range 1150-1300°C, it has been substantiated by subsequent work on anhydrous lunar basalts to pressures of 12 kbar (Walker, Kirkpatrick, Longhi, and Hays, 1975). The water-poor nature of the basalts in this study and their low Fe_2O_3/FeO ratio (Table I) imply that these basalts should be comparable to those used by Roeder and Emslie (1970). However, Mysen (1975), working with water-saturated magmas in equilibrium with natural spinel peridotites under upper mantle conditions, cautions that K_D may decrease with decreasing pressure and increasing temperature. It is possible that the small amount of water in these samples may have affected the partitioning of Fe and Mg between melt and olivine.

In any event, the fact that all olivine crystals, regardless of size, have very similar compositions implies that they were all close

to equilibrium with the enclosing matrix magma just prior to quenching. The similarity of the K_D values is consistent with this conclusion. Yet the well-known ease with which olivines equilibrate to surrounding melt does not permit one to conclude with complete confidence that all of the olivines are cognate. At this point, it can only be stated that there is no evidence to suggest a noncognate genesis for the inclusion-bearing olivines in the glassy pillow rims.

Plagioclase compositions are more variable within individual grains and from grain to grain. Compositionally and texturally, they seem to fall into two basic categories (Table II; Figure 2):

1) phenocrysts (in 10C1 and 4C1) which are anhedral and slightly elongate to equidimensional are distributed evenly throughout pillow rim and interior, exhibit relatively homogeneous, anorthite-rich, interior compositions (An_{80} to An_{86}), and have thin, discontinuous albitic rims (An_{66} to An_{76});
2) tiny, lath-like groundmass microcrysts which are found interior to the glassy pillow rinds are about 2-15μm across and less than 50μm long, with a relatively homogeneous composition similar to or lower in anorthite than the albitic rims of the phenocrysts.

The implication of this textural-compositional evidence is that the homogeneous interiors of the plagioclase phenocrysts approached equilibrium with the bulk magma composition at some time prior to quenching, and that the rims and laths are quench products which do not represent equilibrium crystallization. Substantiating this interpretation is the fact that the rims and laths have a composition which is similar to, or

Table II. Summary of All Data Collected on Plagioclase Compositions.

Sample No.	Normative Min.	PHENOCRYST Avg. (All data)	PHENOCRYST Max. An	PHENOCRYST Min. An	PHENOCRYST No. of data points	GROUND MASS Avg. (All data)	GROUND MASS Max. An	GROUND MASS Min. An	GROUND MASS No. of data points
10C1	Or	0.04	0.04	0.10		0.15	0.10	0.09	
	Ab	15.36	12.26	24.78	60	31.33	28.21	31.31	10
	An	84.58	87.70	75.12		68.52	71.69	68.60	
4C1	Or	0.06	0.05	0.13		0.13	0.10	0.23	
	Ab	22.73	17.72	33.38	37	34.61	32.46	37.75	24
	An	77.21	82.23	66.49		65.25	68.44	62.02	
3A3-2	Or					.11	.10	.13	
	Ab					31.64	29.30	34.26	22
	An					68.25	70.60	56.61	
10C18	Or					.19	.16	.27	
	Ab					37.37	32.51	43.71	19
	An					62.43	65.33	56.02	

identical with, the quenched glass in terms of Ca/(Ca + Na) mole percent (Figure 2). Extending the analogy of the horizontal axis of these frequency diagrams to the compositional axis of a T-X solid solution diagram for plagioclase, the microcryst-glass relationship would correspond to a quenched system in which the temperature is lowered rapidly through the liquidus-solidus interval, so that the crystals and magma have the same composition. In this case, it seems much easier to prove disequilibirum than it is to prove equilibrium. The relatively homogeneous interiors of plagioclase crystals probably record an approach to equilibrium during some unspecified interval in the earlier history of the magma, but there seems no way to unequivocally establish that such a condition existed.

If the homogeneous plagioclase interiors are taken to represent plagioclase formed during an approach to equilibrium at some time prior to quenching, then application of the Mathez (1973) modification of the Kudo and Weill (1970) plagioclase geothermometer may provide temperature estimates corresponding to that equilibrium condition.

Phenocryst-glass pairs from sample 10C1 give temperatures which range from 1285 to 1268°C, and phenocrysts from 4C1 indicate a range from 1232 to 1194°C.

Phenocryst-glass temperatures calculated from well-behaved, linear ln K vs. 1/T relationship derived by Drake (1976) for the reaction $NaAlO_2^{liq} + 3SiO_2^{liq} = NaAlSi_3O_8^{plag}$ in basaltic composition systems, are substantially higher than those determined using the Kudo-Weill-Mathez calculation. Table III compares temperatures for the two approaches

Table III. Plagioclase-glass 'Equilibrium' Temperatures.[1]

Sample No.	Plagioclase Description	Anorthite Component	Temp°C (KWM)[2]	Temp°C (Drake)[3]
3A3	Average of groundmass microcrysts	68.2	1195	1183
4C1	Average of 5 phenocryst interiors	76.6	1204	1340
4C1	Average of groundmass microcrysts	65.3	1203	1190
10C18	Average of groundmass microcrysts	62.4	1151	1140
10C1	Average of 3 phenocryst interiors in glassy rim of pillow	84.7	1268	1448
10C1	Average of 2 phenocryst interiors from pillow interior	85.1	1285	--
10C1	Average groundmass microcrysts near glassy rim	70.5	1215	1179
10C1	Average groundmass microcrysts from pillow interior	65.9	1229	1129

[1]All temperatures were calculated using the composition of matrix glass in glassy rim of pillow. Assumption of equilibrium is probably invalid for groundmass microcrysts.

[2]Temperatures calculated using Mathez (1973) modification of Kudo and Weill (1970) plagioclase geothermometer.

[3]Temperatures calculated using expression $\ln K = \frac{6100}{T} - 2.29$ (Drake, 1976).

using identical mineral-glass pairs. Although the phenocryst values calculated by the ln K vs. 1/T relationship are probably too high, it is curious that application of both geothermometers to the microcryst-glass pairs, which are clearly out of equilibrium, produces very reasonable basaltic magmatic temperatures between 1229 and 1153°C. This situation prompts the caveat that neither geothermometer is sensitive to attainment of equilibrium.

In summary, basalt glasses with inclusion-bearing crystals used in this study fall well within the category of oceanic tholeiitic basalts. They may be considered typical of a vast volume of basaltic magma emplaced in the oceanic crust from the mantle per unit time. While it is not possible to unequivocally establish a cognate relationship between inclusion-bearing crystals and enclosing magma, there is very little evidence to challenge a phenocryst-melt relationship. In fact, the close correspondence between compositions of large and small olivines is evidence that olivine-melt equilibrium was approached prior to quenching. The less reactive plagioclase probably preserves in its interior compositions which were close to equilibrium with matrix magma, although they may not have been at the time of quenching. Assuming the Kudo-Weill-Mathez geothermometer provides valid temperature estimates for systems of the type studied here, magmas 10C1 and 4C1 probably erupted at temperatures between 1200 and 1275°C. The fact that most of the other samples fall within the range between these two (Figure 2) implies that such temperatures apply to other magmas as well.

Glass-Vapor Inclusions in Phenocrysts from Glassy Rims of Pillow Basalts

Previous Work

Rapidly chilled crystalline phases in volcanic rocks commonly contain inclusions of glass (Roedder, 1965; Roedder and Weiblen, 1972, 1973a, 1973b; Anderson and Wright, 1972; Anderson, 1974; Watson, 1976). Many of these inclusions bear volatile phases which have been studied by Roedder (1965); Anderson (1974); Bazarova, Canilho, Sobolev, and Shugorova (1973); and Sobolev, Bazarova, and Bakumenko (1972). The basic premise of most studies is that the inclusions have sampled magma at some depth greater than that of the eruption. Roedder's (1965) observations of liquid CO_2 inside olivines from peridotite nodules indicate entrapment at pressures greater than several kilobars if the system was above 1200°C. However, liquid CO_2 has not been described in inclusions within phenocrysts from oceanic basalts, nor is any evidence of liquid CO_2 found in the samples used in this study.

Anderson (1974) and Watson (1976) assumed that 1) melt initially entrapped in a crystal is chemically representative of the magma from which the crystal grew, and 2) after entrapment, the melt reacts only with the host crystal. Watson (1976, p. 74) specifically states his assumption that "diffusion through the crystal is unimportant in altering the composition of the trapped melt." As discussed later, these assumptions may be valid for major elements and sulfur, but consideration must be given to diffusion of other volatiles during and after crystal growth to establish whether the current volatile content of inclusions is representative of that in the magma at the time of entrapment.

Anderson (1974) estimated the entrapment water content of magma by analyzing glass inclusions in olivine from Mount Shasta using a water-by-difference method on an electron microprobe. He reconstructed initial amounts of magma in inclusions based on textural interpretations of the amounts of post-entrapment growth of the host olivine at the expense of the inclusion. Watson (1976) demonstrated that glass inclusions inside three different phenocryst types from a dredge haul near Bouvet Island in the South Atlantic had reacted with host minerals only, and could be used to establish an earlier composition of entrapped magma. He did not treat volatiles in the inclusions, although he mentions that most inclusions contain a single fluid phase.

Roedder (1965), Sobolev et al. (1972), and Bazarova et al. (1973) report that nodules and phenocrysts in alkali basaltic and kimberlitic lavas commonly contain inclusions with CO_2-rich liquid and minor glass. Roedder also describes very low-density vapor bubbles enclosed within glass inclusions trapped within possible "xenocrysts" in tholeiitic basalts. The bubble usually occupies less than 5% by volume of the total inclusion. He interprets these vapor phases as "shrinkage" features resulting from differential thermal contraction between crystal and trapped magma. Watson (1976) and Anderson (1974), as well as the data presented later in this work, demonstrate that most inclusions have continued to precipitate host mineral after entrapment. Microprobe analyses of plagioclase and olivine crystals containing inclusions imply that the bulk of each phenocryst was close to equilibrium with the enclosing magma now quenched as matrix glass. The inclusions are

considered samples of enclosing matrix magma. As will be developed below, two of the most important textural interpretations deal with the pressures inside the inclusions compared to pressures outside in the matrix glass, and with the question of whether or not inclusions trapped magma only, or magma plus vapor.

Textures of Glass-Vapor Inclusions within Phenocrysts

Most phenocrysts of olivine, plagioclase, and spinel from pillow basalts examined in this study contain some inclusions (Figures 3 and 4). Crystals quenched in the glassy pillow rims contain inclusions which are dominantly glass, apparently quenched with the surrounding matrix magma by eruption onto the ocean floor (Figure 3A). Inclusions in phenocrysts from pillow interiors usually contain partially or completely crystallized material mimicking textures in the enclosing crystalline basalt.

In spite of their common occurrence in rapidly quenched volcanic rocks, glass-vapor inclusions in phenocrysts have not been well described. Because of their potential importance as samples of more "primitive" magma and volatiles, a discussion of petrographic features displayed by these inclusions is worthwhile. The following series of observations and interpretations deals principally with textures found in phenocrysts from the glassy rims of pillow basalts. Inclusions from the rim phenocrysts more accurately record the prequench, magmatic relationships than do inclusions in phenocrysts from pillow interiors.

The size of the glass inclusions is highly variable, ranging from less than 1μm to as much as 1 mm in diameter. Inclusions in olivine

Figure 3. Glass-vapor Inclusions in Plagioclase.

A. Plagioclase (Pc) and olivine (ol) phenocryst quenched in the glassy rim of submarine pillow basalt. Large inclusions of glass (gl) are apparent in plagioclase and smaller inclusions may be seen in the upper right-hand corner of the plagioclase phenocryst.

B, C. Glass-to-vapor (V) volume ratio is relatively constant.

D. Necking between the two lobes implies continued crystallization of the host mineral at the expense of the included magma.

E. Vapor phase was apparently moving toward the top of the photograph at the time of quenching. About 5% of the plagioclase inclusions resemble this irregularly shaped vapor phase. It was not observed in olivine inclusions, probably because they are much less abundant.

F. Unidentified submicron-sized opaque grains lining the glass-crystal interface.

G, H. Low-density vapor phase partly or completely replaced during sample preparation by higher density fluid. These types of inclusions occur dominantly near the surface of any crystal fragment or thin section, and are interpreted to have formed during thin section preparation or crushing.

I. Multiple vapor phases in single glass inclusion. This texture is uncommon in oceanic basalts but is much more common in samples which are richer in volatiles (e.g., Marianas sample).

J. "Elongate" inclusion with "elongate" bubble demonstrates difficulty of measuring volume ratios in some inclusions. The inclusion and the bubble are actually disc-shaped.

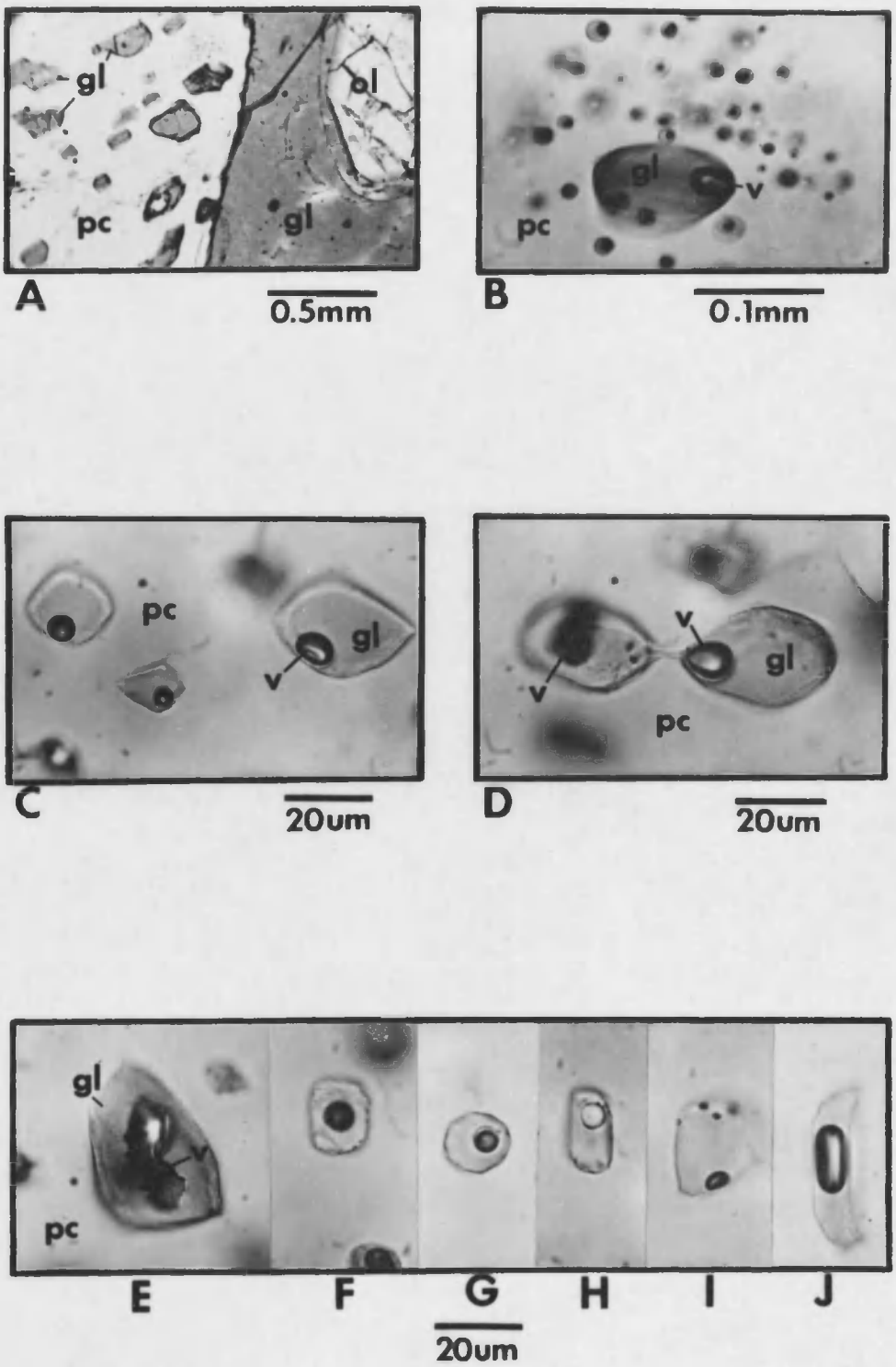

Figure 3. Glass-vapor Inclusions in Plagioclase.

Figure 4. Textures in Glassy Rims of M.O.R. Basalts.

A. Euhedral olivine grain containing a nearly symmetrical series of glass-vapor inclusions. The inclusions appear to record a sequential entrapment process in which the inclusion vapor bubbles develop only after the inclusion is isolated from the matrix glass.

B. Olivine crystal under crossed nicols showing typical glass-vapor inclusions and the correlation between size of vapor phase and the overall inclusion size.

C. Chrome spinel, embedded in plagioclase, containing a vapor-glass inclusion. Inclusions within spinel may represent the deepest available volatile samples.

D. Vapor inclusion embedded in glass partly surrounded by chrome spinel crystal which is completely enclosed within an olivine grain. Crossed nicols.

E. Rare fracture-controlled glass-vapor inclusions in olivine from pillow interior.

F. Rare example of embayed olivine-glass interface photographed under crossed nicols. The interface and embayment appear to have localized vesicles which are contained in the matrix glass. (See text for discussion.)

G. Incompletely formed inclusion of glass and vapor in an olivine grain. The bubble is now partly filled with grinding compound. (See text for discussion.)

H. Degassed inclusion from a plagioclase crystal which has been heated to 1290°C in a vacuum. The irregular pattern surrounding the dark void is glass/magma which "exploded" into a through-going fracture during decrepitation. Volatile loss during this type of event produces very sharp gas release 'spikes'.

I. Glass from a pillow basalt rim with some quench crystals and a vesicle. Embedded in the vesicle wall are sulfide globules similar to those described by Moore and Calk (1971).

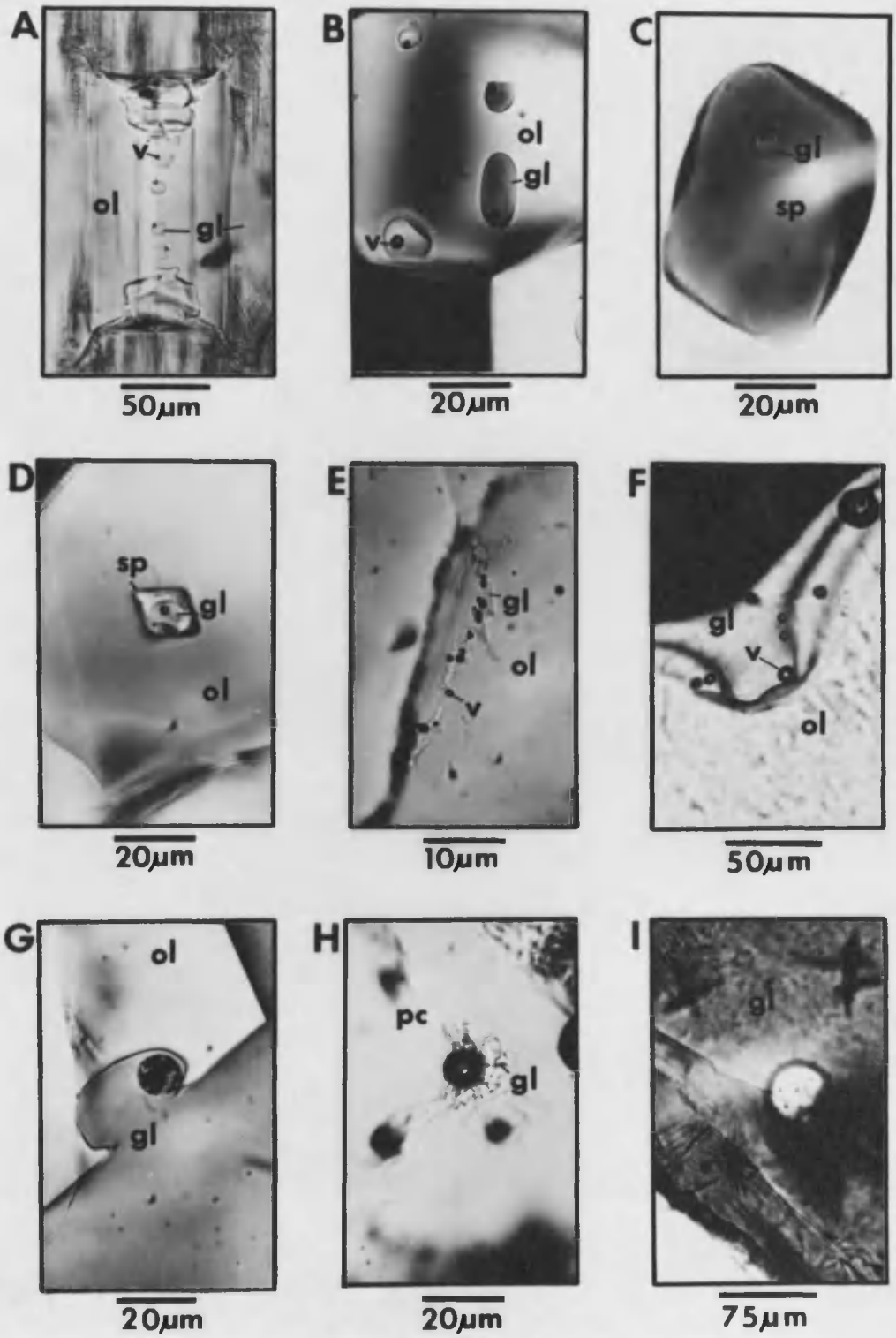

Figure 4. Textures in Glassy Rims of M.O.R. Basalts.

are usually intermediate in size and less abundant than those observed in plagioclase. Some plagioclase crystals have consistently large inclusions (>0.5 mm maximum diameter as viewed in two dimensions); others have predominantly small (<10μm) inclusions, but more frequently, a complete range of sizes is observed in a single crystal (Figures 3A,3B). The shape of the glass inclusions is also variable. In olivine, the inclusions tend to be slightly elongate spheroids, but occasionally crystal-shaped outlines are observed which are glass-filled, euhedrally shaped inclusions in olivine. Large inclusions in plagioclase are irregular to subrounded, and smaller inclusions commonly appear slightly to distinctly elongate in the albite twin plane (Figures 3H,3J). Although variations in shape cause some difficulty in estimating volumes of both glass and vapor, the majority of inclusions resemble those shown in Figure 3C, and volume estimates may be closely approximated by assuming spherical geometry.

Most glass inclusions in plagioclase and many in olivine contain nearly spherical, single-phase fluid inclusions with a very low index of refraction (Figures 3B,3C). A few, small glass inclusions (∿20μm maximum diameter) definitely do not contain a vapor phase, and about 0.5% of the inclusions appear to contain bubbles with a higher index of refraction or appear to be bubble-free. These have been intersected by a fragment surface or thin section surface which has removed or truncated the bubble. Figures 3G and 3H are photomicrographs of vapor inclusions within glass which are close to a thin section surface and have apparently been partially or completely opened to the atmosphere, such

that in 3G a portion of the original vapor is displaced with mounting medium and in 3H the entire vapor phase has been replaced. These types of inclusion are very rare and occur near fractures. Figure 3E shows an irregularly shaped vapor phase similar to about 5% of the inclusions observed in plagioclase. The irregular shape is probably caused by physical movement of the bubble just prior to quenching.

The low-index bubbles are identical to those described by Roedder (1965) as "shrinkage" and "near vacuum" features. Crushing experiments in index oils using the method described by Roedder (1965) failed to produce significant volume expansion upon release of the vapor as the inclusions opened. Crushing of matrix glasses released as much or more gas for equivalent bubble sizes. The pressures within this type of inclusion do not seem high, and are probably under about the same pressure as the vesicles in the matrix glass.

The crystal-glass interface of some glass inclusions within plagioclase is lined with submicron-sized opaque grains of unknown composition (Figure 3F). Vapor-glass surfaces of similar inclusions commonly show slightly larger opaque grains, often with a square cross-section, which are also unidentified (Figures 3G,3H). These may be tiny sulfide grains similar to, but smaller than, those observed lining vesicles in the matrix glass (Figure 4I)(Moore and Calk, 1971; Mathez and Yeats, 1976). However, even if these are sulfide grains, they do not represent a significant amount of additional sulfur compared to that dissolved in the glass.

An important interpretation of the textural evidence is whether or not inclusions entrapped magma alone or magma plus vapor. Unfortunately, some of the evidence is conflicting on this point, but the

post-entrapment evolution of an inclusion will certainly reduce the original entrapment pressure, whether by differential thermal contraction of magma vs. crystal or by continued crystallization of the inclusion magma on the inclusion walls. Figure 3D shows a classic necking feature between two lobes of an originally continuous inclusion. The common interpretation of this texture is continued growth of the host at the expense of the inclusion material. Electron microprobe evidence demonstrates that many inclusions continue to crystallize host material from the entrapped magma. A comparison of the partial molar volumes of the plagioclase and olivine components dissolved in the melt (Bottinga and Weill, 1970) with molar volumes of the same components in a crystalline state at 1200°C (Skinner, 1966) indicates that continued crystallization in an isolated inclusion system would produce a pressure or volume reduction proportional to the reaction progress.

The average diameter of all regularly shaped vapor bubbles in glass inclusions from plagioclase is between one-quarter to one-third the inclusion diameter. Assuming spherical geometry, this corresponds to a bubble volume percent in an inclusion of less than 5%. A very small number of inclusions have either no bubbles or bubbles smaller than the one-quarter diameter and only rarely was a vapor bubble observed larger than one-third of the diameter of the enclosing glass inclusion. For olivine inclusions, the bubble is commonly somewhat smaller for a given volume of glass inclusion than would be the case in plagioclase, possibly reflecting less extensive post-entrapment crystallization for olivines. If inclusions commonly trapped a two-phase magma,

that is, vapor plus magma, then the volume ratio of vapor to inclusion glass should be much more variable than is observed.

Figure 4A shows a quenched olivine grain which preserves the sequence of development of glass-vapor inclusions. In this case, the bubble phase in each inclusion does not seem to develop until the inclusion is isolated from the matrix glass. The consistency of bubble-to-glass volume ratio is also shown in Figures 3B, 3C, and 4B. However, Figure 4F shows an embayment of glass in olivine with vesicles lining the glass-olivine interface. Obviously, if this embayment became an inclusion, the inclusion would contain preexisting vapor-bubbles. Figure 4G shows an inclusion on the margin of an olivine crystal, not yet isolated from matrix glass, which already contains a sizeable vapor bubble (now filled with grinding compound). Yet, more than 2000 inclusions observed display the consistent glass-to-vapor volume ratio, while Figures 4F and 4G are the only cases observed which show the possibility of entrapment of a vapor phase.

Entrapment of vapor bubbles apparently does occur, but it is not common and most inclusions entrap only magma. The vapor phase generally develops after entrapment as a result of differential thermal contraction between crystal and glass (Roedder, 1965) and/or continued precipitation of host crystal on the walls of the inclusion. The possibility that some inclusions may have trapped magma plus vapor raises the intriguing question concerning the depth at which the system became saturated with respect to a vapor phase. However, this is a difficult question to evaluate with samples quenched at the ocean floor where the

magma was obviously volatile saturated as evidenced by about 1% vesicles in most glassy basalt pillow rims. The topic is considered more exten- in a later section.

Chemical Comparisons of Glass-Vapor Inclusions

Electron microprobe analytical data for glass inclusions and matrix glass are presented in Appendix B. Following Watson (1976), these data are illustrated in terms of a triangular diagram in Figure 5. This type of plot permits an approximate evaluation of the evolutionary paths taken by inclusions reacting only with their host mineral. That is, reaction with host minerals which are plotted along the appropriate margin will drive the inclusion chemistry directly away from the host. However, one of the most powerful uses of the "Watson plots" requires that inclusion formation occur simultaneously in all crystallizing phases. Watson (1976) explores the validity of this assumption and the utility of the approach in his analysis of dredged basalts from the vicinity of Bouvet Island in the South Atlantic. Plotting glass inclusions from coexisting plagioclase, olivine, and clinopyroxene, he found a unique intersection of the inclusion fractionation trends which he interpreted to be a more "primitive" magma composition (meaning closer to the original melt composition) than existed within the actual pillow basalt. At the time of quenching, this earlier magma was distinctly more "primitive" (lower TiO_2 and higher Mg/Fe) than the quenched matrix magma which surrounds the inclusion-bearing phenocrysts. In other words, it may be misleading to compare inclusions directly with matrix material

Figure 5. Triangular MgO-CaO-Al_2O_3 Diagrams Showing Matrix and Inclusion Glass Microprobe Analyses. -- Major phases precipitating from a magma may be plotted as weight percent oxide on the margins of the diagram. Crystallization of any one phase would drive the remaining liquid in a unique direction. Inclusions trapped during such a process could record the path but also react with the host mineral. Two relatively primitive magmas, one from Watson (1976) and one from Frey, Bryan, and Thompson (1974) are plotted in Figure 5B to demonstrate the low TiO_2 and high Mg/Fe ratio of such magmas. Data for two samples are plotted in Figure 5A; R1-24 data are in the lower half of the diagram and data for 2A1 in the upper half.

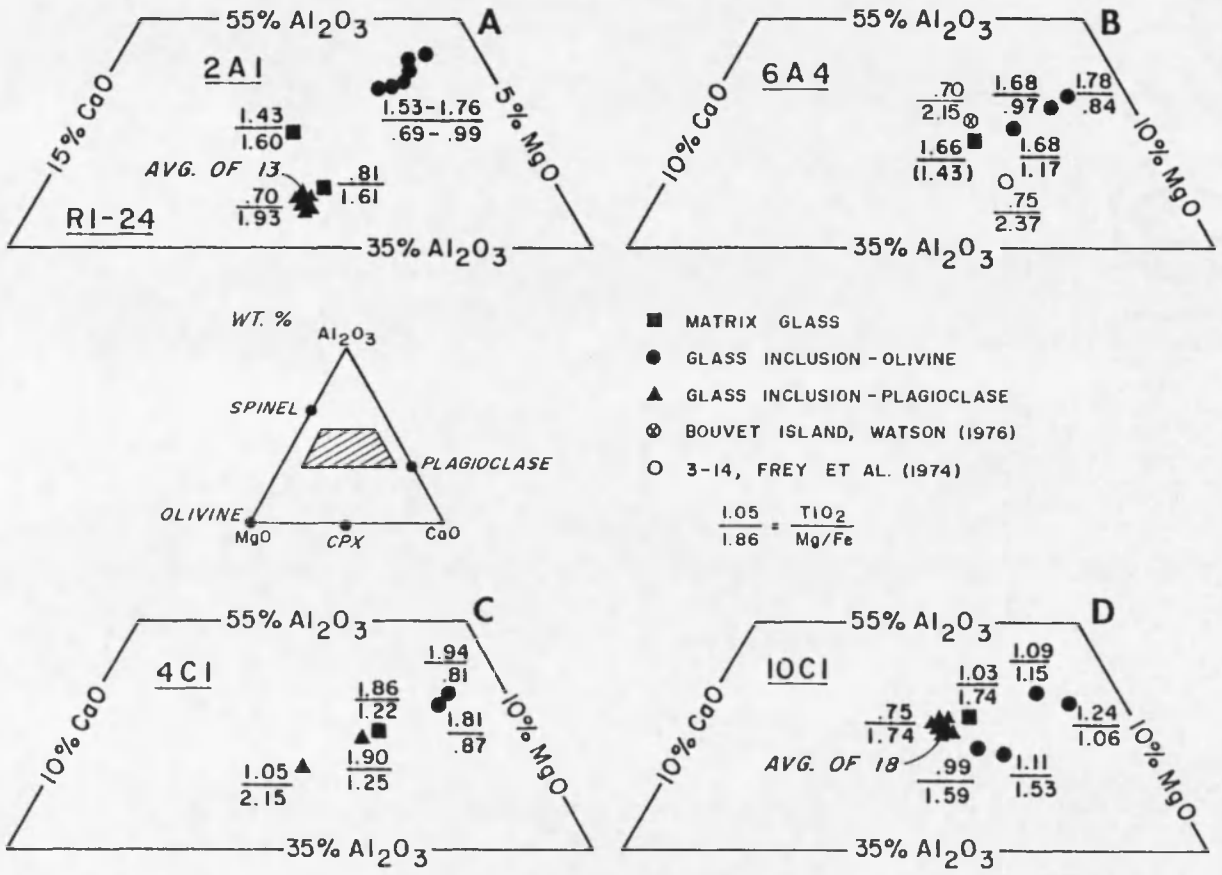

Figure 5. Triangular MgO-CaO-Al_2O_3 Diagrams Showing Matrix and Inclusion Glass Microprobe Analyses.

to interpret the extent of post-entrapment inclusion evolution. This is because a significant amount of post-inclusion entrapment crystallization can modify the matrix composition substantially, making it less "primitive" than trapped inclusions which have interacted solely with the host mineral. If the inclusions were not formed as a result of a single event, then a unique solution is not possible. However, certain elements of the system's evolution may still be established.

Most glass samples in this study contain only plagioclase and/or olivine. Inclusions and matrix glass from samples 4C1, 10C1, R1-24, 6A4, and 2A1 are plotted in Figure 5. The pair of numbers (index ratio) adjacent to the plotted points show weight percent TiO_2 in the numerator and mole ratio of Mg/Fe in the denominator for each sample. Also shown in Figure 5B, for comparison, are the TiO_2 and Mg/Fe values of two relatively primitive seafloor basalts. These are taken from Watson's reconstruction of the Bouvet Island Suite and from Frey et al.'s (1974) data on sample 3-14 from the Deep Sea Drilling Project. Both magmas are characterized by very low TiO_2 (<0.80 wt %) and a high Mg/Fe ratio (~ 2.1); any magma with similar values may be considered "primitive". TiO_2 content of a magma increases and Mg/Fe decreases with continued fractional crystallization.

In the case of 2A1 and 6A4, the glass inclusions in olivine have evolved from the matrix composition essentially by precipitation of olivine. Both TiO_2 and Mg/Fe values suggest that the matrix composition is differentiated, and the glass inclusions appear even more differentiated than the matrix. However, inclusions in plagioclase from samples R1-24

and 10C1, and one inclusion from 4C1 retain relatively low TiO_2 values and fairly high Mg/Fe ratios. Plagioclase inclusions from sample R1-24 are perhaps the most "primitive" based on criteria cited above, and 10C1 plagioclases seem not to have evolved far either. Both sets of inclusion data from R1-24 and 10C1 are clustered near the matrix glass values, and the index ratio of inclusions and matrix is similar, indicating the rocks themselves have not evolved much since entrapment of inclusions. These data are interpreted to mean that the inclusions have trapped relatively primitive magma which had not evolved significantly by fractionation prior to or after inclusion formation.

Conversely, inclusions in 4C1 plagioclase samples two distinct stages of magma evolution, one of which had a TiO_2/(Mg/Fe) value of 1.05/2.15 and the other a value of 1.9/1.25, which is similar to the matrix glass. Some plagioclase sampled primitive magma, while later plagioclase sampled magma resembling the present matrix glass which has evolved significantly since early plagioclase growth. Inclusions in olivines from 4C1 closely resemble the matrix glass in terms of TiO_2, probably having been entrapped late in the system's history.

Olivine glass inclusions from 10C1 are more difficult to interpret than any other sample. It is not possible to establish a unique explanation for them. The matrix glass has a consistently higher TiO_2 content than the more "primitive" plagioclase inclusions. Yet the position of the matrix is <u>above</u> the fractionation line connecting plagioclase composition and the glass inclusions. Therefore, the matrix glass must have previously been located somewhere on the fractionation line. The

two MgO-poor glass inclusions in olivine may be explained in terms of olivine fractionation from a more primitive magma previously located along the plagioclase join. However, the other two glass inclusions in olivine, with relatively high Mg/Fe ratios, must have either been trapped very early or did not significantly react with the host olivine. Alternatively, if the two glass inclusions in question contained microcrystals of spinel, the present arrangement might have been produced. No such inclusions were observed, but grinding of the probe mount may have removed them.

Mathez's (1976) study of sulfur solubility in submarine basalt glasses demonstrated a linear covariance between total Fe and S dissolved in 34 matrix glasses from a wide variety of locations. He was also able to establish that sulfur concentrations within inclusion glasses from phenocrysts were generally similar to, or slightly greater than, sulfur concentrations of matrix glass. Figure 6 is a plot of wt % sulfur vs. wt % TiO_2 for 12 seafloor basalt samples with glass inclusions inside phenocrysts quenched in matrix glass. The most important point to be demonstrated from these data is the relative ease with which the sulfur content of glass inclusions within phenocrysts can be statistically characterized. Regardless of whether the glass inclusions are within plagioclase or olivine, they generally cluster about and somewhat above the sulfur content of the matrix glass. The principal exceptions are most of the inclusions in R1-24 (Kolbeinsey Ridge) and one of the inclusions in 4C1 (1.05 wt % TiO_2). These inclusions have distinctly less sulfur and distinctly less TiO_2 than the matrix magma, and may represent magma

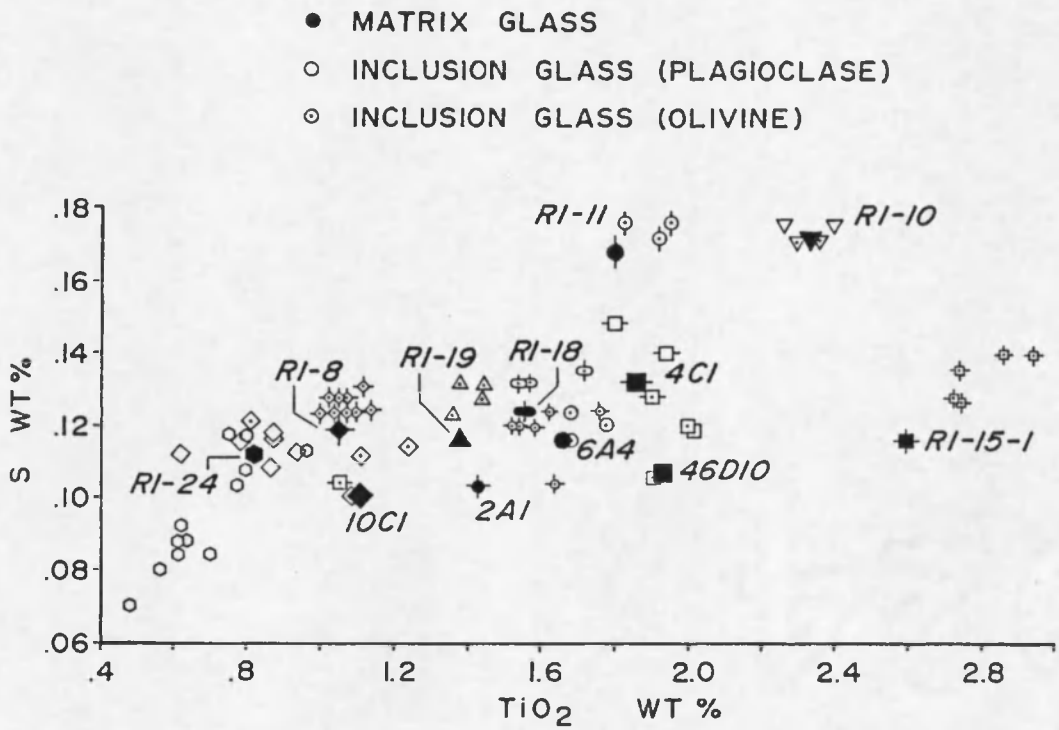

Figure 6. Weight Percent Sulfur vs. Weight Percent TiO_2 for Electron Microprobe Analyses of Matrix and Inclusion Glasses. -- See text for discussion.

trapped at an earlier (deeper?) stage of magma evolution. The trend of increasing TiO_2 with increasing S in R1-24 plagioclase inclusions may record a concommitant enrichment of the two elements during fractional crystallization. If so, the sample with lowest sulfur and TiO_2 may have been trapped at the deepest level, and may contain more CO_2 than other inclusions analyzed. These types of relationships open the intriguing possibility that the volatile evolution of a magma may be traced through careful analysis of specific glass inclusions. Unfortunately, at this time it is not possible to analyze individual inclusions for water and CO_2. A second point is that the consistent clustering of inclusion glass compositions in terms of TiO_2 and sulfur values strongly supports the assumption that the crystalline phases are phenocrysts, not xenocrysts.

In summary,

1) Plagioclases from R1-24 and 10C1 seem to have sampled relatively primitive magma;
2) Some of the plagioclase from 4C1 sampled "primitive" magma and some sampled much less "primitive" material;
3) Olivines from 10C1 may also have sampled relatively primitive magma, but it is not as obvious as with the plagioclase inclusions;
4) Olivines in 2A1, 4C1, and 6A4 appear to have sampled magma indistinguishable from the matrix glass;
5) A small amount of clinopyroxene fractionation and/or combined precipitation of olivine and plagioclase must account for the

present composition of matrix glass with respect to R1-24 and 10C1 inclusions in plagioclase;

6) The sulfur content of glass inclusions does not generally differ significantly from that of the matrix glass.

7) The clustering of inclusion glass about matrix glass substantiates the Mathez (1976) conclusion that the inclusions are samples of the matrix, thereby solving the dilemma of phenocryst or no.

DEGASSING EXPERIMENTS

The quenched glassy rims of the MORB basalts and the phenocrysts with glass inclusions were degassed separately to determine the volatile contents of the matrix and included glasses. The details of the experimental techniques are as follows.

Sample Preparation

Glassy portions of pillow basalt rims were chipped away from the rock sample and crushed in a stainless steel mortar and pestle. A size fraction of the sample of 1.0 to 0.2 mm diameter was cleaned in an ultrasonic vibrator with doubly distilled water to remove all crushing powder and most of the palagonitic alteration. Glass and phenocrysts were then hand picked under a binocular microscope. Glass fragments with spherulites, visible crystals, and alteration of any type were rejected. Several glass samples still contained 1 to 2% by volume of microphenocrysts completely enclosed within a glass fragment. However, the total volatile content of the glass is significantly higher than an equal volume of crystals which usually contain less than 1% by volume inclusion glass with less than 0.4% volatiles. The microcrysts act essentially as a diluent in the glass. Phenocryst fragments of olivine and plagioclase were partly concentrated using a magnetic separator, and then hand picked. Again, any fragments with visible alteration or iron-staining were rejected. The only visible non-crystalline components were glass-vapor inclusions

within the phenocrysts. Considerable care was taken to exclude phenocryst fragments with matrix glass adhering to the outer surface.

Each sample was immersed in 0.3N HCl solution for two hours to remove any carbonate film which might have formed on fracture surfaces. Several samples were analyzed which had not been treated with HCl and little difference was observed, implying that carbonate was not a serious contaminant (cf. Pineau, Javoy, and Bottinga, 1976). Rewashing in doubly distilled water and drying for two hours at 120°C completed initial preparations for degassing.

High-Temperature Mass Spectrometry

Instrumentation

The volatile content and degassing behavior of all samples was obtained with a high-temperature mass spectrometric facility consisting of an effusion-vaporization source interfaced with a computer-controlled quadrupole mass spectrometer (a modified EAI, Quad. 1110). The effusion assembly contains a molybdenum Knudsen cell heated by radiation from a coiled tantalum resistance element. A set of concentric cylinders surround the cell and serve as a radiation shield and beam collimator. Details of the vaporization source have been previously described by Muenow (1973). From this source a molecular beam of released volatiles is generated. It emerges through an orifice in the cell lid, and is then directed through a movable shutterplate and into the ion source of the mass spectrometer. An important feature of this arrangement is the short, direct line-of-sight placement between the ion source and cell orifice.

Use of the shutterplate allows distinction between molecular species emitted directly from the Knudsen cell and those re-emitted and scattered from other surfaces of the system. The mass spectrometer is controlled by a PDP/1145 computer. Temperature is measured with a Pt/Pt-10% Rh thermocouple peened into the base of the cell, and is also controlled by computer. The high-temperature unit is contained within a water-cooled housing, and pumped with a high through-put, fast-cycling vacuum system (to 1×10^{-8} torr) containing sublimation and ion pumps.

Techniques and Procedures

Two basic types of degassing experiments were conducted: 1) rapid-scan mode in which many masses are monitored by rapidly cycling spectrometer, and 2) fixed-mass mode in which one mass can be continuously monitored by focusing the spectrometer on that mass. For the glass samples the mass spectrometer was operated in a rapid-scan mode to obtain mass pyrograms (quantitative gas release profiles) using the procedures of Killingley and Muenow (1975a). Samples were weighed and placed into a prebaked Lucalox (crystalline high-temperature alumina) cell liner and heated under a vacuum of 1×10^{-8} torr at a rate of approximately 5°/min to 1250°C. During this time the mass spectrometer rapidly scans the spectrum from 1 to 150 amu (or any other pre-selected mass range). Ion-current signals for all mass peaks and temperatures are measured and stored on magnetic tape. Gas species identification was based upon appearance potentials, fragmentation patterns, and isotopic abundances. Mass pyrograms are then obtained as hard-copy computer plots of the intensities of parent molecular ions (or principal fragment ions) versus

temperature. Those used for quantitative evaluation of the total volatile content are obtained when the product of the "corrected" ion-intensity and the square root of the absolute temperature is plotted against the absolute temperature. The "corrected" ion-intensity is the measured ion-intensity adjusted for system background, fragmentation, isotopic abundance, relative ionization cross-section, electron multiplier efficiency, and quadrupole transmission effects. System background contributions are determined by use of the shutterplate and from "blank" runs made before and after each sample study. For each mass curve of the 150 masses scanned, approximately 140 data points are obtained. When degassing of each glass sample is completed, the sample is allowed to cool and then is reweighed. Weight loss is entered as computer input for a final check on the calculation of absolute volatile abundances lost.

The sensitivity of the mass spectrometer was determined by the calibration procedure based on the quantitative vaporization of a known amount of a standard substance (Grimley, 1967). The standardization procedure is carried out routinely and is considered acceptable when the measured heat of fusion from the standard material matches values published by the National Bureau of Standards within the uncertainty of these values. This procedure assures stability of all instrumental components and establishes that quantitative vaporization is achieved and that there is no significant loss between the effusion cell and the mass spectrometer. For these studies, a .1 mg sample of high-purity magnesium metal serves as the standard.

For degassing phenocryst samples, measurements were made by operating the mass spectrometer in a switchable fixed-mass mode, as well as the rapid-scan mode, to obtain mass pyrograms. By continuously monitoring a major ion mass of any volatile of interest (or several, by periodically switching from mass to mass), it is possible to observe rapid changes in the ion intensity as sharp spikes on a fast-response, strip-chart pen recorder and an oscilloscope. These spikes could not be adequately recorded by the rapid-scan technique. For minerals containing volatile-bearing inclusions, the ion current signal spikes appear at high temperature and correspond to vapor release from one or a number of ruptured inclusions. This phenomenon has previously been observed for CO_2-release from fluid inclusions in olivine separated from dunitic and perioditititic nodules (Killingley and Muenow, 1974). It is believed to be the result of cracking caused by stresses due to temperature gradients within the olivine grains (Killingley and Muenow, 1975b).

The spiked-release character of the phenocryst degassing curves precludes the integration approach used with matrix glass curves to establish quantitative volatile contents in the inclusions. For quantitative measurement of volatile spiking, an instrumental calibration is accomplished with the aid of tiny glass ampules containing known volumes of CO_2 (Killingley and Muenow, 1975b). More important, in terms of the present study, is the fact that within the mass range of interest (<100 amu), instrumental sensitivities for various species differ by no more than a factor of four (D. W. Muenow, personal communication, 1977); that is, if the system detection limit can be established for one of the

species, then a maximum detection limit for other species can be established. The use of ampules with known amounts of CO_2 can then be used to place limits on the sensitivity of the instrument for all volatile species of interest. To this end, the CO_2-bearing ampules are heated in the Knudsen cell until they burst, releasing their contents. Recorder spike-heights corresponding to these standards are plotted against known CO_2 content. When the CO_2 content of the ampules is below 1×10^{-14} mole, spiking activity drops below background for CO_2 (Killingley and Muenow, 1975b). Considering variations in relative sensitivity and background for different species and conservatively allowing a variation of ½ order of magnitude instead of a factor of 2, the detection limit of the instrument for spiked release of the volatiles CO_2, H_2O, and SO_2 is at least 5×10^{-13} mole per recorder spike. This means that spiked release of less than 5×10^{-13} mole of any of these species could just be lost in background, but that release of more than 1×10^{-11} gram (5×10^{-13} mole) of H_2O or 3×10^{-11} gram of SO_2 per spike event would produce a measurable response. This detection limit is an important figure, as it is used later to place a limit on the amount of water in the glass-vapor inclusions.

Phenocryst sample size varied from 12 to 300 mg. Glass-vapor inclusions occupy from less than 0.5 to 10 volume-percent of the phenocryst samples. Each sample was heated at 5°/min to 1300°C and monitored throughout for its vapor burst-release behavior.

Results

Matrix Glass

Degassing patterns of the principal volatiles, CO_2, H_2O, and SO_2 from glasses 2A1, 3A3, 4C1, 6A4, 7A4, 10C1, 10C4, and R1-24 are presented in Figure 7A and B. Detailed analysis of each curve may eventually provide information about the site occupancy of volatiles in the glasses. The major features of the 3A3 pyrogram are typical of mass pyrograms obtained for many of the glasses studied (2A1, 3A3, 4C1, 6A4, 7A4, R1-18). Most glasses release small amounts of water and display small CO_2 spikes between 700 and 800°C, followed by major water-release peaks at 930 ± 30°C. Glasses 10C1, 10C4, and R1-24 release distinctly larger amounts of H_2O at about 760°C and display broader, lower water-release peaks between 900 and 960°C. Water has been completely removed from all samples by 1000°C. Neither increasing temperature to 1400°C nor subsequent heating cycles induces additional water loss. In contrast, a mass pyrogram of the interior, crystalline portion of a pillow basalt is characterized by a very broad water-release peak which is well developed at 150°C, reaches a maximum about 210°C, and gradually tapers to 1400°C (Figure 8). The implication of this water-release pattern for the glass is that the water is structurally bound to the alumino-silicate 'lattice' of the melt, and is, therefore, much more fundamentally important in the igneous petrologic interpretation of magma behavior than water which is commonly reported as H_2O^+ in most standard rock analyses. The gentle, positive slope of the glass degassing curves for water beyond about 1120°C is system background, and does not reflect sample degassing activity.

Figure 7. Mass Pyrograms for Matrix Glass. -- Intensities are normalized to 100% in the region of greatest gas release. Samples 2A1, 3A3, 4C1, 6A4, and 7A4 differ from samples 10C1, 10C4, and R1-24, in which the bulk of the water from the sample is released below 800°C. In all of the samples studied, water is completely released by 1000°C, and CO_2 and SO_2 are degassed by 1100°C. The solid lines are for water release, the dashed lines are for CO_2, and the dot-dash lines represent SO_2 release. All three volatiles are plotted at the same scale of ion intensity.

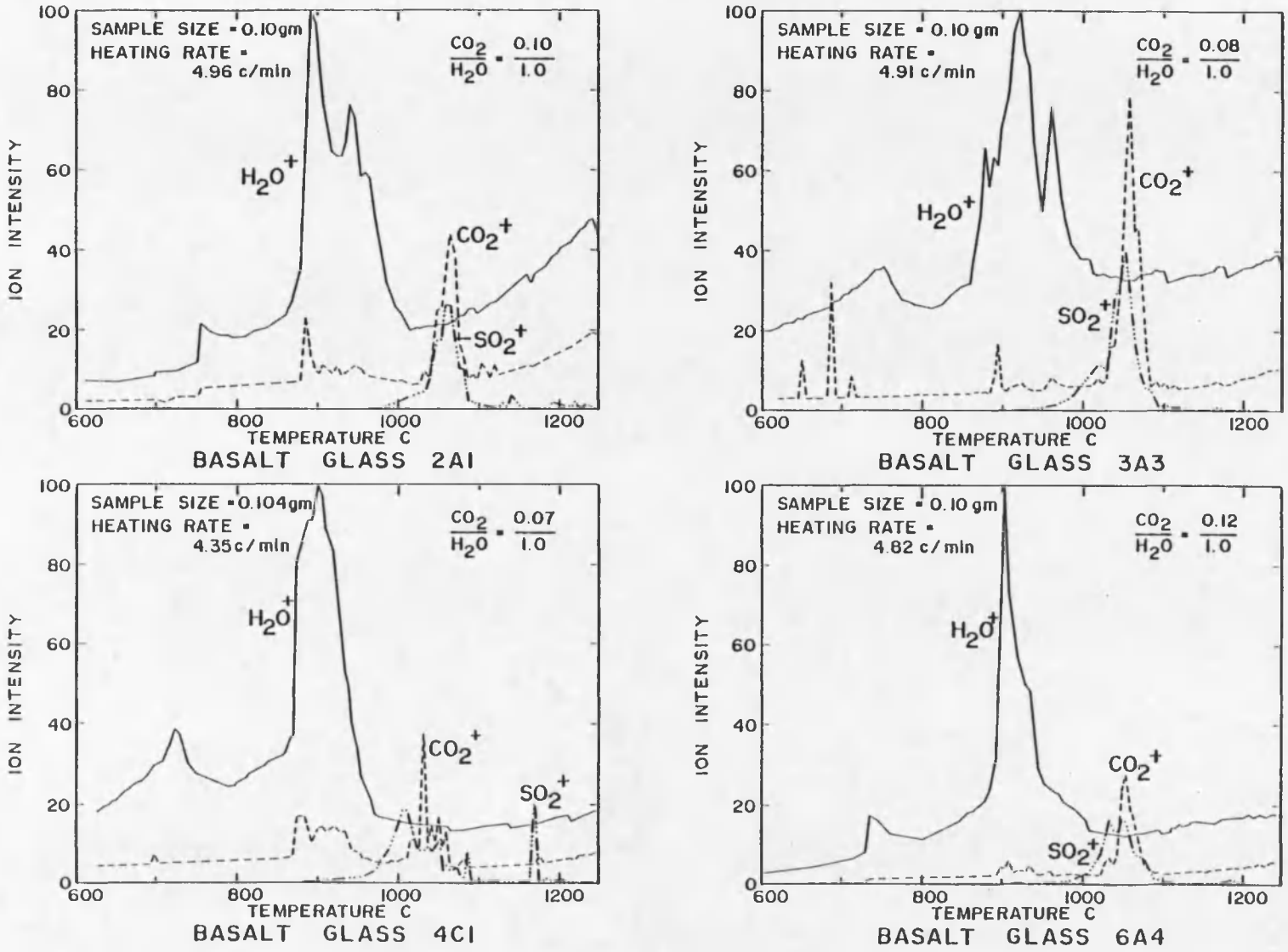

Figure 7. Mass Pyrograms for Matrix Glass. -- A. Samples 2A1, 3A3, 4C1, 6A4.

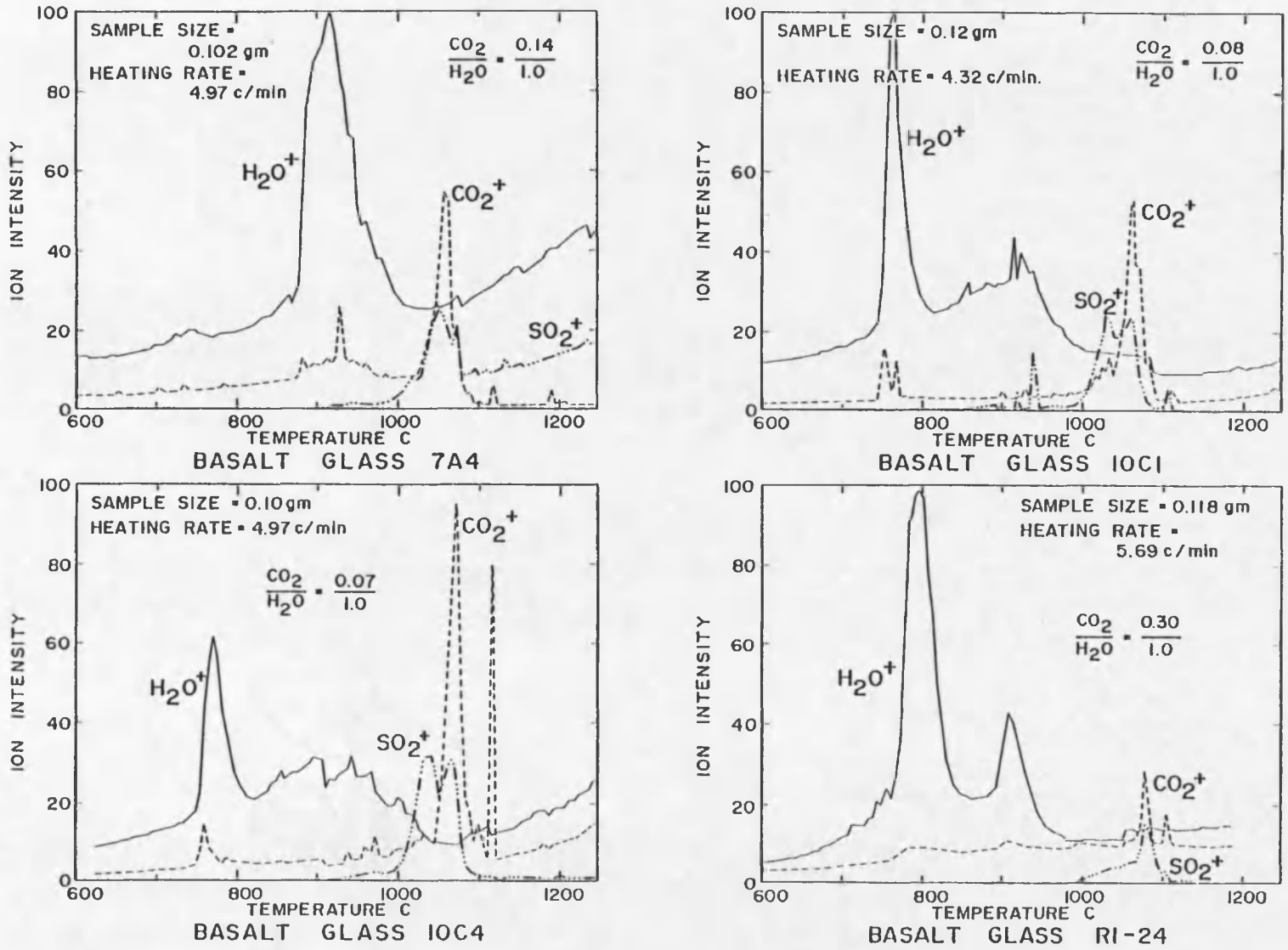

Figure 7, continued. -- B. Samples 7A4, 10C1, 10C4, R1-24.

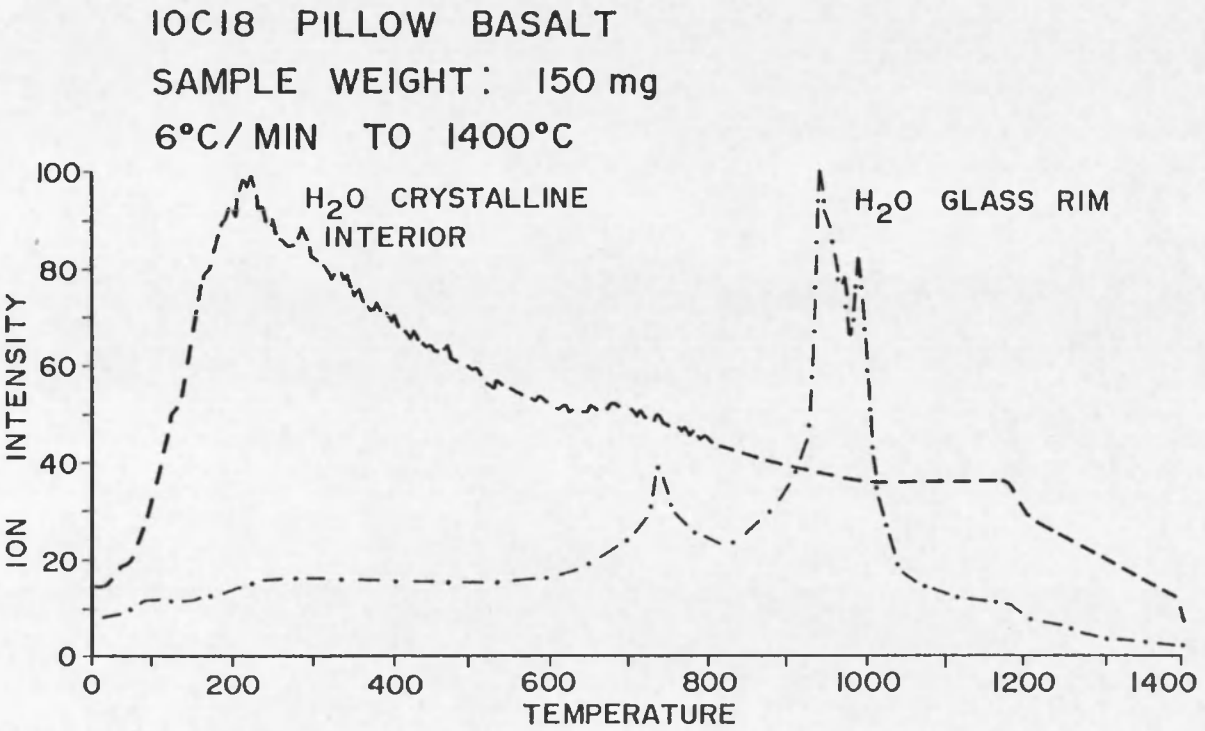

Figure 8. Comparative Mass Pyrograms Showing Water Release from Glassy Rind and from Crystalline Interior of Pillow Basalt. -- The peak height at the point of maximum water release is arbitrarily assigned a relative ion intensity of 100. Standard rock chemical analyses reporting H_2O^+ and H_2O^- would clearly give ambivalent results for crystalline interiors as regards water content related to the original magma.

Concurrent with the second water peak in the matrix glass samples, a small amount of CO_2 is consistently released. However, most of the CO_2 and SO_2 are lost from the sample between 1020 and 1090°C. The CO_2- and SO_2-release curves have distinct, consistent, and sharp maxima which correlate closely to each other in all samples studied.

At least two mass spectrometeric analyses were made for each of the glasses studied. Differences in mass pyrograms for replicate samples were minor. Weight losses are essentially due to release of the volatiles H_2O, CO_2, and SO_2. Minor components are Cl, F, and O_2. Small mass peaks for Na and H_2S molecules are also observed at temperatures above 1200°C. These probably result from decomposition of the glass and the gas phase reaction of released sulfur with background water vapor. Species identification was based upon appearance potential measurements and isotopic abundance.

The specific mechanisms of volatile release are not well understood, but the consistency of the release temperatures is useful in discussing the degassing curves of phenocrysts quenched in the rims of some of these samples. It is important to note that the degassing process is essentially an artificially induced phenomenon that bears little similarity to any natural process of degassing.

Although a detailed analysis of the thermal gas-release curves was not a major objective of this study, several comments are in order.

1) The low-temperature (650-750°C) CO_2 spikes, seen best in 3A3 glass and found in several other samples at low temperatures, probably represent opening of CO_2-rich vesicles in the matrix

glass as a result of initial softening. They do not always occur in replicate runs, and apparently depend on distribution and size of vesicles in the fragments selected for analysis. Notably, there is no sympathetic response in the H_2O or SO_2 curves, implying that the volatile content of the vesicles under the conditions of degassing is principally CO_2.

2) Water-release peaks for most of the samples at 750 $\pm$ 20°C may also be related to this softening process, but apparently do not derive from vesicle opening, since the gentle slopes of the low-water peaks do not show the sharp, spike-type release associated with vesicle opening.

3) The larger water-release peaks at about 930 $\pm$ 30°C in samples, 2A1, 3A3, 4C1, 6A4, 7A4, and R1-18, representing the final and major water loss from these samples, seem to correspond to an incipient devitrification. Petrographic and electron microprobe examination of samples heated in a vacuum to 1000°C and then quenched, show very little of the original clear, brown glass, but show many large, irregularly shaped vesicles, and an erratic distribution of sulfur.

4) The significance of a major water-release peak at about 750°C for samples 10C1, 10C4, and R1-24 is not obvious at this point. All three glass samples which display the low-temperature major water release peaks are strongly porphyritic with plagioclase, and 10C1 and 10C4 contain abundant olivine and minor spinel. All three glass samples have relatively low (<1.0 wt %) TiO_2 contents.

Otherwise they do not seem to differ from the glasses with a higher-temperature, major water-release peak.

5) Loss of SO_2 and CO_2 corresponds to melting of the samples. At 1140°C, the samples behave as liquids, the vesicles are well-rounded, and by that temperature, the sulfur content of residual glass is below the detection limit of the electron microprobe (about 100 ppm) and less than 80 ppm by Leco analysis (Appendix C).

6) With continued heating to 1250°C and quenching, the samples again become clear, brown glass virtually devoid of volatiles or vesicles, although optically similar to the original glass.

Phenocrysts with
Glass-Vapor Inclusions

Mass pyrograms for all plagioclase and olivine samples show no significant degassing behavior below 1000°C. These include olivines from MAR 10C1, 10C4; Juan de Fuca R1-8; Explorer Seamount R1-18; Paul Revere Ridge R1-3; Hawaii SBO-5; Marianas-21-D-1; and plagioclases from MAR 10C1, 10C4, and 4C1; Kolbeinsey R1-24. At approximately 1020°C, CO_2 and SO_2 begin to spike, indicating burst-release of the corresponding volatiles (cf. Killingley and Muenow, 1974). There is no indication of water loss from most of the phenocrysts during this burst-release behavior.

Since only one mass may be continuously monitored at any given time, periodic mass switching is necessary to monitor all masses showing burst-release behavior. Pyrograms obtained in this manner consist of a series of temperature intervals during which degassing activity of various

masses is recorded. Figure 9 shows selected temperature segments from an actual pyrogram in the continuous monitoring mode. Multiple experiments for the phenocrysts demonstrate the same number of both CO_2 and SO_2 spikes for similar temperature intervals; that is, the release of CO_2 corresponds to the release of SO_2. Maximum burst-release behavior of CO_2 and SO_2 from olivine samples of 12-80 mg takes place in the range 1070-1150°C; for similar-sized plagioclase samples, spiking reaches its maximum in the range 1040-1120°C. Samples with larger grain sizes tend to exhibit spiking behavior over a larger temperature interval than samples of equal mass but smaller grain size. Weak spiking activity was observed in several samples at temperatures as high as 1250°C, and for one 300 mg plagioclase sample, with fragment grain sizes as large as 2.5 mm diameter (R1-24), spiking continued to 1300°C and was also induced upon quenching. The phenomenon of gas release upon quenching has been investigated in olivines by Killingley and Muenow (1974, 1975b). Plagioclase fragments virtually free of inclusions failed to produce significant spiking, whereas vigorous spiking was observed under identical conditions in plagioclase fragments from the same sample that had nearly 10 volume percent inclusions.

This evidence indicates that the spiking corresponds to bursting events of one or more glass-vapor inclusions. Figure 4I shows an inclusion after the sample (R1-24) had been heated to produce a mass pyrogram (Figure 9).

An important point is that the spikes represent the combined release of volatiles from the vapor bubble as well as gas dissolved in the

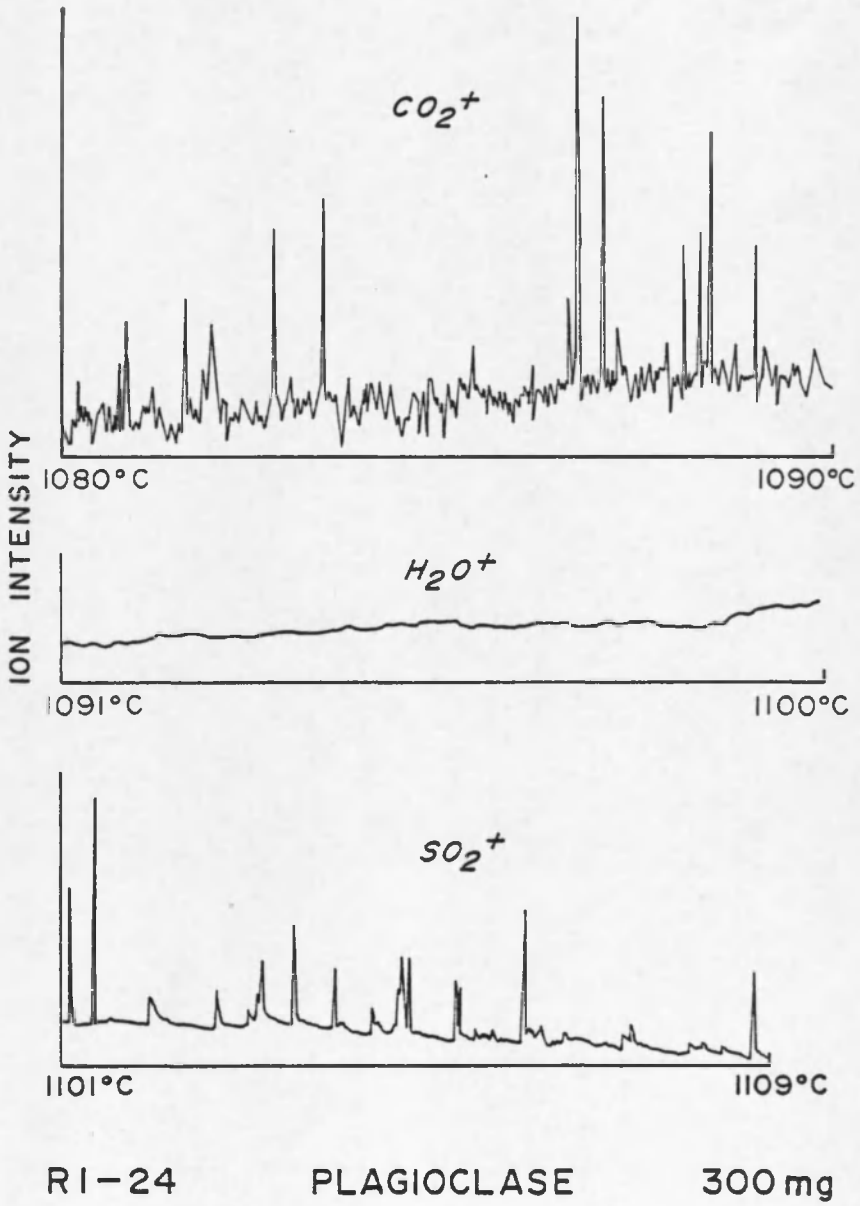

Figure 9. Plagioclase Phenocryst Mass Pyrogram. -- Temperature segments of a mass pyrogram in the fixed-mass, continuous-monitoring mode with periodic switching to show gas release behavior of important volatile species. This sample contained 300 mg of plagioclase phenocrysts from the glassy rim of sample R1-24. Note the complete lack of water response.

glass portion of the inclusion. Apparently when the inclusions burst at temperatures greater than 1000°C and suddenly are exposed to a vacuum (10^{-10} atm), the total volatile content of the inclusion is released. Petrographic examination of the degassed crystals indicates that up to 50 burst inclusions may occur along a single fracture. Re-quenched glass is commonly spread irregularly along the fracture plane. The nearly spherical volume originally occupied by the glass-vapor inclusion prior to degassing is now an open void (Figure 4I), apparently resulting from eruption of the original inclusion contents into the fracture plane at the time of spiking. The number of spikes per pyrogram is normally much less than the total number of inclusions observed to have been opened. This fact and the presence of so many degassed inclusions along fractures can only mean that individual spiking events often represent degassing of numerous inclusions.

CO_2:H_2O Ratio. Measured background, instrumental noise levels, and sensitivities permit conservative estimates of absolute minimum CO_2:H_2O mole ratios for all other phenocryst sets to be fixed at 30:1. This value is established by assuming the water signal is just buried in background, and compares to a mole ratio of CO_2:H_2O <0.15 found in all matrix glasses of oceanic basalts. By contrast, a pair of phenocryst sets--olivine and plagioclase--in the glassy rind of a fresh submarine tholeiite from the Marianas Interarc Basin exhibited vigorous spiking of water along with similar spiking activity for CO_2 and SO_2. Measured ion intensities permit a rough estimate for the CO_2:H_2O mole ratio of about .4/1.0 for the glass-vapor inclusions. The petrologic significance of

the Marianas sample will be discussed elsewhere, but the principal value of the data at this point is to demonstrate that: 1) inclusions can retain water (this point is discussed extensively in the next section), and 2) the mass spectrometer easily detects water when it is present.

Upper Limit of Water Content. The single most important observation of this study is the apparent low water content of the glass-vapor inclusions within phenocrysts from open-ocean basins. Placing a realistic limit on the maximum water content of the inclusions is of considerable significance to the major conclusions of this work.

Trapped inclusion glass and the surrounding matrix glass should display similar degassing phenomena since they have similar major- and minor-element (including sulfur) compositions (Figures 5, 6; Appendix B). The temperature at which spiking from the inclusions is initiated corresponds closely to the temperature at which CO_2 and SO_2 begin to degas from the surrounding matrix glass (Figure 10). Yet water, the dominant volatile component of the matrix, would be completely dispelled from the matrix glass well below spiking temperatures. Therefore, if the inclusions contained measurable water, it should certainly be available for degassing when the spiking events occur. But none is observed. To test the possibility that water or hydrogen might have leaked out of the inclusions along fractures or flaws prior to spiking, large samples of inclusion-bearing phenocrysts were carefully monitored for H_2O and H_2 from 600°C to the initiation of spiking. No sample degassing of any sort was detected. In addition, the vigorous water signal observed in phenocryst samples from the Marianas demonstrates that the inclusions can

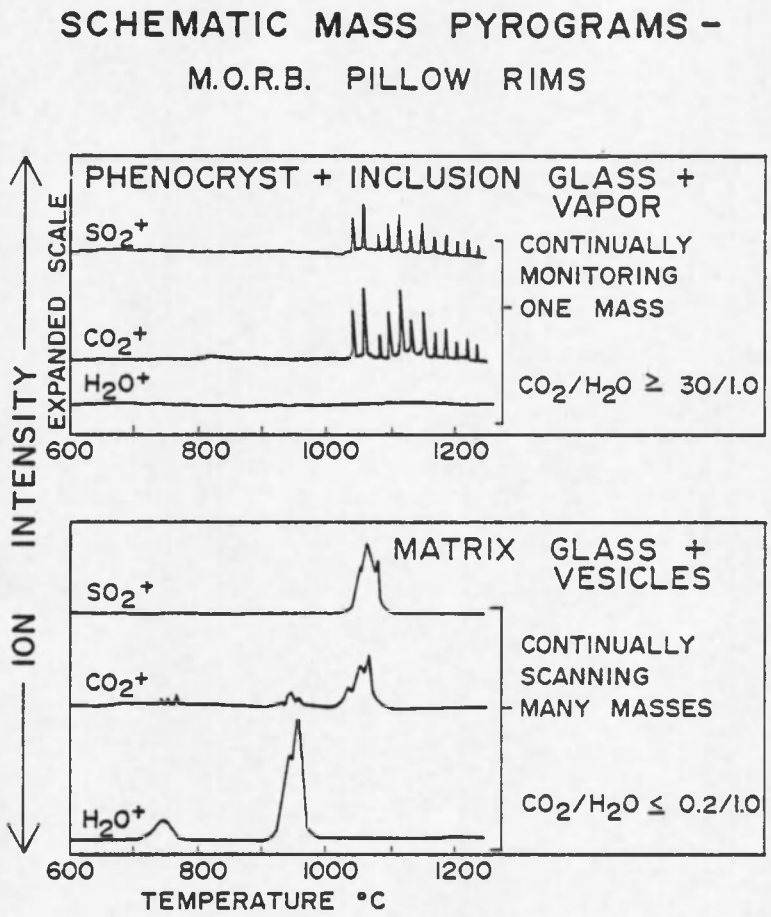

Figure 10. Schematic Mass Pyrograms for Typical M.O.R.B. Pillow Rims. -- Top--Phenocryst pyrogram showing spiking for CO_2 and SO_2 with no detectable H_2O. Bottom--matrix glass pyrograms showing typical volatile release pattern. Spiking activity for the phenocrysts begins at the temperature range of maximum CO_2 and SO_2 release from the matrix glass.

retain water until spiking begins. Therefore, if water is released from open-ocean basalt phenocrysts, it is below the detection limit of the mass spectrometer.

Previous discussion (p. 46) concluded that the sensitivity of the instrument for H_2O is 1×10^{-11} grams using the spiked release, fixed-mass monitoring mode. Any spiking event in which less than this amount of gas is released could be lost in background signal. To place an upper limit on the amount of water in the inclusions, it is assumed that the water spike is <u>just</u> lost in the background signal (that is, that 1×10^{-11} gm H_2O per spike <u>is</u> released). The average amount of glass which would be involved in a spiking event would be an average single inclusion, which is used to compute the mass of H_2O per mass of inclusion glass.

Using the expression:

$$\frac{\text{Mass } H_2O \text{ detectable}}{\text{Spike event}} \div \frac{\text{Average mass of a glass inclusion}}{\text{Spike event}} = \frac{\text{Mass } H_2O}{\text{Mass glass}} \quad (1)$$

an inclusion of 70μm diameter is taken as an average mass of glass which contributes to a spike. Many inclusions larger than 70μm were degassed, and petrographic evidence indicates that a single fracture may intersect 10 to 100 degassed inclusions. Replacing the small volume occupied by the vapor phase with glass, the mass of a spherical inclusion is given by:

$$\text{Mass of inclusion glass} = (4/3\ \pi r^3)\rho = 4.6 \times 10^{-7} \text{ gm glass/inclusion} \quad (2)$$

where r is the radius of sphere (35μm) and ρ is the approximate density of glass in an inclusion (about 2.6 gm/cc). Equation (1) gives a value

of 2.2×10^{-5} gm H_2O/gm glass or .002 wt % water. This figure is considered to be an upper limit to the concentration of H_2O in inclusion glass, because no water was ever detected in the open-ocean basalt phenocrysts, and some of the spiking events must have represented considerably larger masses of degassing inclusion glass than the average inclusion used in this computation.

Estimation of CO_2 Content. It is not now possible to identify the actual number or size of inclusions which contribute to a specific spike. Therefore, the concentration of CO_2 in the inclusions cannot be established using the CO_2 ampule calibration curve mentioned earlier (p. 46). At this time, estimates of inclusion CO_2 content can only be made on a statistical basis using large numbers of spikes, providing only average values for inclusions. The following is a description of the approach and assumptions.

Heating large samples of phenocrysts (>100 mg) produces numerous spikes, and by switching between masses 44 (CO_2^+) and 64 (SO_2^+) it is possible to establish an average spike height for CO_2 and SO_2 released. Since the fragmentation patterns and background levels of these two gases are similar, the spike heights are proportional to the total amounts of carbon and sulfur gases released (D. W. Muenow, personal communication, 1977). Ratios of the average spike heights approximate the average molar ratios of the two gases released from the samples. The 300 mg sample of R1-24 produced over 500 spikes, providing an opportunity to alternately monitor the two masses throughout the range of burst-release behavior and

thereby establish an average CO_2/SO_2 molar ratio which was about 3. Most of the phenocryst samples analyzed have similar spike ratios, but because of its size, R1-24 offered the most statistically valid sample and, therefore, the most precisely measured ratio. The relative size of the CO_2 and SO_2 spike heights did not change significantly throughout the degassing sequence.

The average CO_2 content of the inclusions could be estimated if the average sulfur released from the inclusions during spiking were known. Microprobe analyses (Figure 6) show that the average sulfur content of inclusion glass in R1-24 is about 0.09 to 0.1 wt %, or about 0.0031 mole (based on a hypothetical 100 gm sample of inclusion glass). This, of course, represents only the sulfur dissolved in the inclusion glass, but abundance calculations show that this is more than 90% of the total inclusion sulfur content, even if the submicron-sized opaque grains are sulfides. Assuming this concentration of sulfur were released during a spiking event, the C/S ratio of 3 would indicate an average carbon content of about 0.01 mole or about 0.4 wt % CO_2.

To test the hypothesis that inclusion sulfur is fully degassed, electron microprobe analyses of degassed samples were run, and no detectable sulfur was found. However, this is a difficult analysis to perform, as most of the degassed inclusion glass is now spread along fractures less than 1μm wide. Alternatively, the degassing curves for matrix glasses indicate that virtually all sulfur is gone from the sample by 1100°C. If this holds true for inclusion glass degassing, then spikes above 1100°C should represent quantitative sulfur degassing.

Statistically, no difference between SO_2 spikes above 1100°C and below 1100°C was observed; so the quantitative degassing of sulfur from inclusions is considered a good assumption. However, if as little as one-half of the sulfur in the inclusion glass is released upon spiking, the average CO_2 content of inclusions would be 0.2 wt %, which is still distinctly higher than the CO_2 content of the matrix glasses. The value of 0.4 wt % is probably too high, but it seems reasonable to propose that in spite of the many assumptions involved in this estimation, the CO_2 content of the inclusions is two to four times greater than the enclosing matrix glass.

Briefly summarizing, the most important conclusion reached in this section is that the glass-vapor inclusions contain much less water (<0.002 wt %) than the enclosing matrix glass (about 0.25 wt %). A more tentative conclusion is that the inclusions contain somewhat more CO_2 than the matrix glass.

INTERPRETATION OF VOLATILE DISTRIBUTION AND ABUNDANCE

Information developed in the previous sections on the distribution and abundance of volatiles in the C-O-H-S system is summarized in Table IV. The striking difference in volatile content between inclusions and matrix glass raises the following questions. Do inclusions preserve the volatile composition of the magma in which they are formed? Have the inclusions been significantly modified with respect to their CO_2 and H_2O contents during and/or after entrapment? If the inclusion-bearing phenocrysts had grown in a magma resembling matrix glass, then concentration of CO_2 at the crystal-magma interface during crystal growth could have enhanced the CO_2 content of the inclusions. Post-entrapment diffusional loss of water (as hydrogen?) through the enclosing phenocrysts might then reduce the water content of the inclusion glass to produce the observed volatile distribution and abundances. If, on the other hand, the magma in which the inclusion-bearing phenocrysts grew had compositions similar to that of the present inclusion composition, then the matrix magma must have lost CO_2 and gained water after inclusion entrapment and before quenching. A third possibility is that the inclusions grew from a magma with a volatile composition intermediate between inclusions and matrix glass, such that the inclusions were enriched in CO_2 and depleted in water, while the matrix magma was depleted in CO_2 and gained water. It is of considerable geochemical and petrologic importance to establish which of these three alternatives is most realistic.

Table IV. Summary of Data on Volatile Distribution and Abundance in Glassy Rims of Oceanic Pillow Basalts.[a]

Sample	MATRIX GLASS				PHENOCRYST			
	H_2O[b] (wt %)	CO_2[c] (ppm)	S[d] (ppm)	CO_2/H_2O (mole ratio)	Phase Analyzed[e]	CO_2/H_2O[b] (mole ratio)	Max. H_2O[b] in Inclu. (wt %)	Location
2A1	0.24	590	1170	.10	---	---	---	MAR
3A3	0.26	480	1200	.08	---	---	---	MAR
4C1	0.26	470	1410	.07	Pc	>30(2)	<.01	MAR
6A4	0.16	480	1350	.12	---	---	---	MAR
7A4	0.26	920	1420	.14	---	---	---	MAR
10C1	0.24	500	970	.09	Pc	>30(2)	<.01	MAR
					Ol	>30	<.01	MAR
10C4	0.21	400	1380	.07	Pc	>30(2)	<.01	MAR
					Ol	>30	<.01	MAR
10C18	0.18	350	1425	.08	---	---	---	MAR
R1-3	0.12		1000		Ol	>30	<.01	PRR
R1-8	0.10		1200		Ol	>30	<.01	JFR
R1-18	0.20		1200		Ol	>30	<.01	FS
R1-24	0.28	350	1100	.08	Pc	>30(4)	<.01	KR
SBO-5	0.58		935		Ol	>30	<.01	Hawaii
21-D-1	2.40				Pc	∿.4	≫.01	Marianas

[a]See Appendix C for description of analytical methods of volatiles in matrix glass.
[b]Mass spectrometric analysis
[c]Leco total carbon analyzer
[d]Best combination of Leco total sulfur analyzer, mass spectrometer, and electron microprobe.
[e]Phenocrysts degassed; Pc = plagioclase, Ol = olivine.

CO_2 Diffusion during Crystal Growth

Inclusions sample magma adjacent to growing crystal faces. As the crystal rejects some magmatic components, concentrations of more slowly diffusing, "rejected" components may be localized near the crystal-magma interface by relatively rapid crystal growth. Incorporation of this magma could produce inclusions enriched in "rejected" components. Carbon dioxide enrichment of the inclusions may be a consequence of such a phenomenon. However, in no way could an imbalance between crystal growth and diffusion rates lead to depletion of the inclusions in "rejected" components. The observed water-poor character of the glass inclusions relative to the matrix glass must be accounted for by some other mechanism(s).

Lack of diffusion data for CO_2 in basaltic melts makes it difficult to evaluate whether the CO_2 enrichment of the inclusions is a kinetic phenomenon or represents an originally higher CO_2 concentration in the matrix magma. It is not even possible to state whether CO_2 diffuses more or less rapidly than water. Yet for several reasons this problem is one of considerable interest. The absolute abundance of CO_2 within inclusions represents a potential geobarometer. That is, the pressure-dependent experimental solubility relationships for pure CO_2 in basaltic magma (Khitarov and Kadik, 1973) indicate a monotonically increasing CO_2 concentration as a function of pressure to at least 3 kb under isothermal conditions. Therefore, if the CO_2 content of an inclusion has not been kinetically enriched to the point of vapor saturation prior to entrapment, the CO_2 concentration of the entrapped magma can be calculated from the

present CO_2 content of the inclusion and from the extent of post-entrapment host mineral growth inside the inclusion. The latter might be estimated using the method of Watson (1976). This CO_2 content, if completely dissolved in the magma during trapping, could give a minimum pressure of entrapment. Furthermore, if sea-floor basalts contained substantially more CO_2 at some earlier stage of evolution, then the CO_2 flux into the oceanic crust from the mantle may be considerably larger than previously recognized. Unfortunately, with data now available it is not possible to discard the hypothesis that CO_2 enrichment of the inclusions was caused by diffusional contamination of the crystal-magma interface during rapid crystal growth.

Diffusion after Inclusion Formation

If the nearly anhydrous character of the glass-vapor inclusions in phenocrysts resulted from diffusional loss of H_2O (or hydrogen) through the enclosing crystal, the chemical potential (μ) of H_2O or hydrogen must have been higher in the entrapped inclusions than in the matrix at some earlier stage. The chemical potential of a component in any system is a function of pressure, temperature, and the bulk composition of the system. However, theoretical computations have demonstrated that for geologically reasonable undercooling there is no significant heat accumulation along the crystal-magma interface during crystal growth (T. P. Loomis, personal communication, 1977); therefore, it is unlikely that a significant temperature difference exists between the inclusion and matrix glass. Electron microprobe analyses indicate that the bulk

chemical compositions of the two glasses do not seem sufficiently different (Appendix B) to produce a significant chemical potential gradient to drive diffusion. Notably, the present distribution of water between inclusion and matrix glass reflects a chemical potential gradient, hence a diffusional driving force for water, toward rather than away from the inclusions. However, the H_2O content of the matrix glass might have been enriched by interaction with hydrous portions of the suboceanic crust at a time when diffusion of water through the inclusion-bearing phenocrysts was too slow to produce any significant effect. If water escaped from the inclusions it must have done so in response to a chemical potential gradient caused by pressure differences between the inclusion and the magma. Melt entrapped in a phenocryst might not have equilibrated with the load pressure during decompression at the same rate as the enclosing matrix magma because of inadequate pressure transmission through the host crystal. Thus, the inclusions might remain at a higher pressure than the surrounding magma. That crystals can sustain significant pressure differentials is evident from Roedder's (1965) descriptions of liquid CO_2-bearing olivines in ultramafic nodules erupted at about 1200°C. Pressure differences between inclusions and matrix of more than 3 kb must have existed at the temperature of eruption.

Instead of using the rather sketchy kinetic data on diffusion of H_2O (or hydrogen) through crystals at 1200°C, the following equilibrium approach permits evaluation of the limit to which H_2O could be depleted by diffusional loss in response to a pressure-induced chemical potential gradient. This is done by assuming diffusional equilibrium between

inclusion and matrix can rapidly be achieved and by calculating the equilibrium distribution of water between inclusion and matrix as a function of pressure differential. The advantages of this approach are that it maximizes the argument for diffusion by assuming equilibrium and it is independent of diffusional mechanisms.

Diffusion of any component i between inclusion and matrix magma must cease when

$$\mu_i^I = \mu_i^M, \tag{1}$$

where μ_i is the chemical potential of component i and the superscripts refer to inclusion and matrix magma. The chemical potential of water in a magma is given by

$$\mu_{H_2O}^{magma} = \mu_{H_2O}^{+}(P,T) + R\ T\ \ln a_{H_2O}^{magma} \tag{2}$$

where a stands for activity and $\mu_{H_2O}^{+}(P,T)$ is the chemical potential of water in magma at some arbitrarily chosen standard state at the given P and T. We define $\mu_{H_2O}^{+}(P,T)$ as the chemical potential of water when the magma is saturated with respect to H_2O, in the absence of any other volatile species, at the P and T concerned. Combining (1) and (2), we have, at equilibrium with respect to diffusion of H_2O between inclusion and matrix,

$$\mu_{H_2O}^{+(I)}(P_I,T_I) + R\ T\ \ln a_{H_2O}^{I} = \mu_{H_2O}^{+(M)}(P_M,T_M) + R\ T\ \ln a_{H_2O}^{M} \tag{3}$$

Since $a_{H_2O} = X_{H_2O}\,\gamma_{H_2O}$, where X_{H_2O} is the mole fraction of H_2O in the system and γ_{H_2O} is the activity coefficient of H_2O in the melt and because $T_I = T_M$, rearrangement of (3) yields

$$R\,T\,\ln\left(\frac{X^I_{H_2O}}{X^M_{H_2O}}\right) = \mu^{+(M)}_{H_2O}(P_M) - \mu^{+(I)}_{H_2O}(P_I) + R\,T\,\ln\left(\frac{\gamma^M_{H_2O}}{\gamma^I_{H_2O}}\right) \qquad (4)$$

It is also true that

$$\left(\frac{\partial \mu^+_{H_2O}}{\partial P}\right)_{T,X} = \bar{V}^+_{H_2O},$$

where $\bar{V}^+_{H_2O}$ is the partial molal volume of H_2O in the magma at the standard state. Since inclusion and matrix glass are very similar with respect to their non-volatile constituents (Figures 5,6; Appendix B) and because temperature was identical for both magmas

$$\mu^{+(M)}_{H_2O}(P_M) - \mu^{+(I)}_{H_2O}(P_I) = \int_{P_I}^{P_M} \bar{V}^+_{H_2O}\,dP. \qquad (5)$$

It will be assumed that $\gamma^M_{H_2O}$ and $\gamma^I_{H_2O}$ differ only as a result of the difference in P_M and P_I and that the activity coefficients are not influenced by compositional differences, other than water, between inclusion and matrix. Thus,

$$R\,T\,\ln\frac{\gamma^M_{H_2O}}{\gamma^I_{H_2O}} = \int_{P_I}^{P_M}\left(\frac{\partial \ln\gamma_{H_2O}}{\partial P}\right)_{T,X} dP + \int_{X^I_{H_2O}}^{X^M_{H_2O}}\left(\frac{\partial \ln\gamma_{H_2O}}{\partial X_{H_2O}}\right)_{P,T} dX_{H_2O} \qquad (6)$$

The maximum water content in the matrix glasses is less than 0.4 wt % justifying use of Henry's Law approximation for the activity coefficient of H_2O in the magma; that is, $\gamma^{M}_{H_2O} \approx$ constant.

As a consequence, the last term in (6) becomes negligible. From (2), it follows that

$$\left(\frac{\partial \ln \gamma^{magma}_{H_2O}}{\partial P}\right)_{T,X} = \frac{\bar{V}^{magma}_{H_2O} - \bar{V}^{+}_{H_2O}}{RT} \quad . \tag{7}$$

Where $\bar{V}^{magma}_{H_2O}$ is the partial molal volume of water in the magma, combining (4), (5), (6), and (7)

$$\ln\left(\frac{X^{I}_{H_2O}}{X^{M}_{H_2O}}\right) = \frac{1}{RT}\int_{P_I}^{P_M} \bar{V}^{+}_{H_2O} dP + \frac{1}{RT}\int_{P_I}^{P_M} (\bar{V}^{magma}_{H_2O} - \bar{V}^{+}_{H_2O})\, dP,$$

which reduces to

$$\left(\frac{X^{I}_{H_2O}}{X^{M}_{H_2O}}\right) = EXP\left[\frac{1}{RT}\int_{P_I}^{P_M} \bar{V}^{magma}_{H_2O}\, dP\right] \tag{8}$$

Equation (8) relates the equilibrium mole fraction of water in the magma at one pressure to that of water in the magma at another pressure assuming that 1) temperature is constant, 2) all components other than water do not influence the activity of water, 3) the Henry's Law approximation holds. The last two should be particularly valid assumptions in view of the low abundance of water. The equilibrium expression is independent of diffusional mechanisms and provides a maximum equilibrium of diffusional loss, in that it is unlikely that diffusional equilibrium is achieved, since diffusion tends to be slow and self-arresting.

Figure 11 shows the relationship between mole fraction ratio $X^{I}_{H_2O}/X^{M}_{H_2O}$ and the two other variables, P_I, the inclusion pressure, and P_M, the confining pressure on the overall system (matrix magma) at equilibrium. Implicit in this diagram is the assumption that the mole fraction ratio was equal to 1.0 at entrapment. Implicit in the following discussion is the assumption that diffusion is not effective after quenching at the ocean floor. Calculations were made by integrating the empirical equation of state for $\overline{V}_{H_2O}$ in an albite melt (Burnham and Davis, 1974) with respect to pressure, at 1200°C. This temperature is higher than the data interval upon which the equation is predicated; however, the function is well-behaved and this should introduce no difficulty. Nor does the use of an equation for albite melt instead of basalt melt significantly influence the results. Burnham and Davis (1974, p. 939) note ". . . for most silicate melts of interest which are predominantly oxygen ions by volume, $\overline{V}_{H_2O}$ (or rather $\overline{V}_{OH^-}$) should be virtually independent of cation composition within wide limits . . .."

Inspection of Figure 11 shows, as expected, that maximum water loss from inclusions would be achieved by maximum pressure differential. The upper diagram also shows that slightly more water should be lost at lower confining pressures than at higher values of P_M. This is important because the P_M isobar for the earth's surface represents a limiting depletion at any ΔP, and because all of the samples solidified under pressures greater than 1 bar. Thus, if an inclusion formed at about 12 km depth and maintained an internal pressure of about 4000 bars as it rose to the surface, it could lose a maximum of 0.6 of its original water

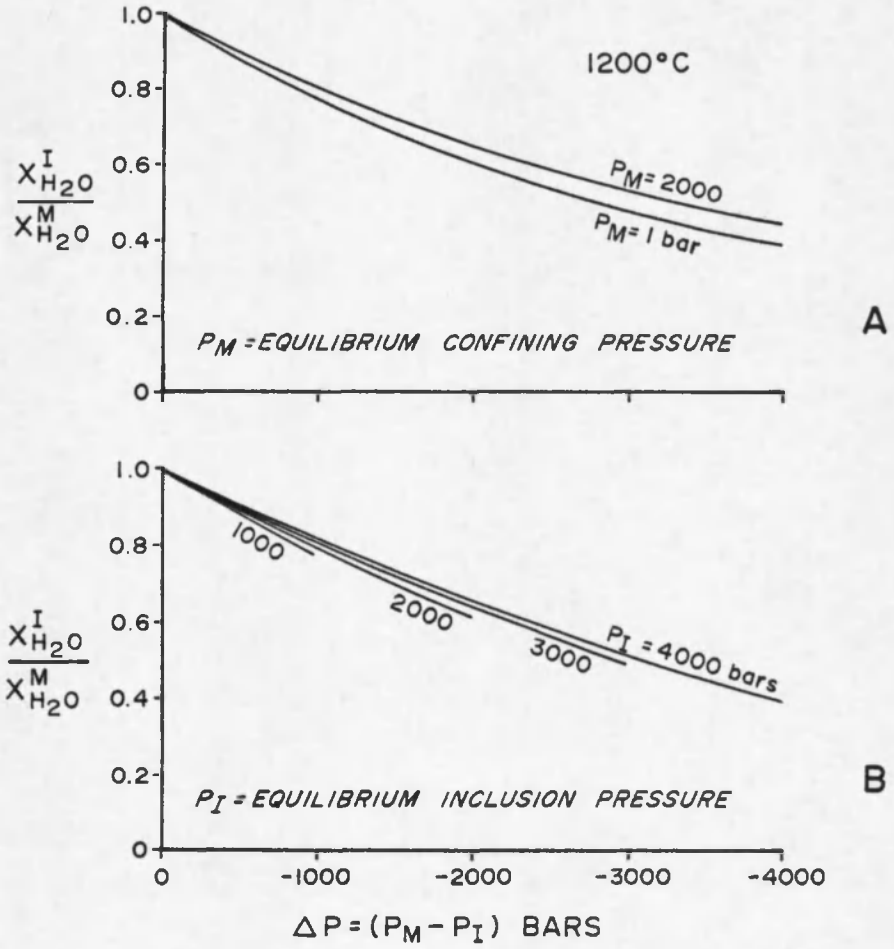

Figure 11. Calculated Equilibrium Mole Fraction Ratio of Water $X^I_{H_2O}/X^M_{H_2O}$ as a Function of Pressure Differential (P_M-P_I) between Inclusion and Matrix Magma at 1200°C. -- The upper diagram has curves for constant confining pressure (P_M) and the lower diagram shows curves of constant inclusion pressure (P_I). See text for derivation and discussion.

assuming osmotic equilibrium with the matrix magma was achieved. The actual path of this simple decompression scheme may be traced in the lower diagram of Figure 11. Beginning at $\Delta P = 0$ and a mole fraction ratio of 1.0 (the conditions of inclusion closure) a specific isobar corresponding to the initial depth may be followed as a limiting depletion case until the system reaches the surface, where ΔP is essentially P_I. This is a limiting condition because as developed earlier (see section on Texture and Chemistry of Inclusions) the inclusion undergoes its own decompression which may be largely independent of the overall confining pressure.

Inclusion decompression would result from at least two causes.

1) The negative ΔV of reaction by which the inclusion magma precipitates host mineral on inclusion walls would decrease the total pressure in the inclusion, and
2) Differential thermal contraction between magma/glass and crystal would also reduce internal pressure.

While both mechanisms would favor vapor saturation, the first would also increase the relative volatile content of the residual liquid, increasing the tendency to form a vapor phase. Since virtually all inclusions contain vapor phases, in about the same vapor-to-glass volume ratio, most of the bubbles must have formed after entrapment. Inclusion decompression, therefore, helped to nucleate bubbles and indicates that nearly all inclusions must have followed a shorter, more gently sloping P_I path (Figure 11B) than would be indicated if the inclusion maintained the pressures corresponding to the actual entrapment depth. The fact that inclusion bubble formation took place demonstrates that the vapor pressure of the

magma in the inclusion exceeded the confining pressure on the inclusion. The fact that no liquid CO_2 was found places an upper limit on that confining pressure.

The section on textures discusses the low pressure nature of the inclusions at room temperature as indicated by the low refractive index, and the single-phase character of the fluid "bubble". Roedder (1965) has described fluid inclusions in olivines from peridotite nodules that contain liquid-gas plus glass inclusions in which the fluid is dominantly CO_2. Upon crushing under immersion oils, the volatiles in these liquid-gas inclusions exhibit a pronounced volume expansion of as much as 300 times the entrapped fluid volume. Crushing of the inclusions in the present study produced no noticeable volume expansion and the inclusions must now be of a low pressure nature. In fact, Roedder (1965, p. 1749) describes the type of inclusion dealt with in the present study as follows: "Ordinary glass inclusions in the minerals of volcanic rocks normally show an immobile 'gas' bubble formed on cooling as a result of greater shrinkage of the glass (magma) than of the surrounding host mineral. Such bubbles are usually found to be nearly a vacuum, and show a relatively constant and small volume ratio to the glass; they were seen in most of the samples investigated." While it is unlikely that the inclusions are near-vacuum, and the bubble is almost certainly the result of continued crystallization of inclusion material as well as the "shrinkage" factor, it seems inescapable that at the time of quenching ΔP was not large. The pressures cited by Roedder (1965) as necessary to entrap sufficiently dense CO_2 at $1200^{\circ}C$, to produce liquid CO_2 at room

temperature, are from 2500-5000 bars. Clearly, those pressures represent an absolute limit on the pressures of the non-liquid CO_2 inclusions of this study. A 5000 bar pressure differential could have produced a five-fold depletion of the original inclusion water content and represents a generously conservative estimate of potential water loss. The limiting estimate in the previous section indicates a maximum present value of 0.002 wt % H_2O in inclusions; therefore, the original water content of the inclusions could not have been more than 0.01 wt %.

Volatile Abundance-- Interpretation and Speculation

Figure 12 shows pressure-dependent solubility curves for the individual species, CO_2 and H_2O, in a basaltic magma below 4 kbars pressure. It is assumed that, at the low pressures and volatile concentrations involved for basalts on the ocean floor, these curves approximate the actual solubility for both gases in the magma, although Mysen (1976) has demonstrated that at high pressures (20 kb) under vapor-saturated conditions the two gases influence each other's solubility. The relatively broad crosshatched solubility limit for CO_2 is the best data currently available for silicate melts in the pressure range depicted, and encompasses experimental uncertainties (Khitarov and Kadik, 1973). Also plotted in Figure 12 are the concentrations of CO_2 and H_2O measured in the matrix glass and the CO_2 compositional range inferred for the inclusions. Notably, since the inclusions are nearly anhydrous the pure CO_2-basalt solubility curve applies without qualifications.

Figure 12. Saturation Curves for Individual Volatile Species in Basaltic Magma. -- The CO_2 curve is from Khitarov and Kadik (1973). The width of the curve is the uncertainty of the experimental data. The water curve is from Hamilton et al. (1964) extrapolated to 1 atm according to a square root pressure dependence (Burnham and Davis, 1971). The matrix glass CO_2 content seems to approximate the saturation of CO_2 for basaltic magma at the pressures on the ocean floor, but H_2O is significantly undersaturated. If the water-poor inclusions were not vapor-saturated at the time of entrapment, a minimum depth of formation may be established if the CO_2 content of the inclusions were accurately known.

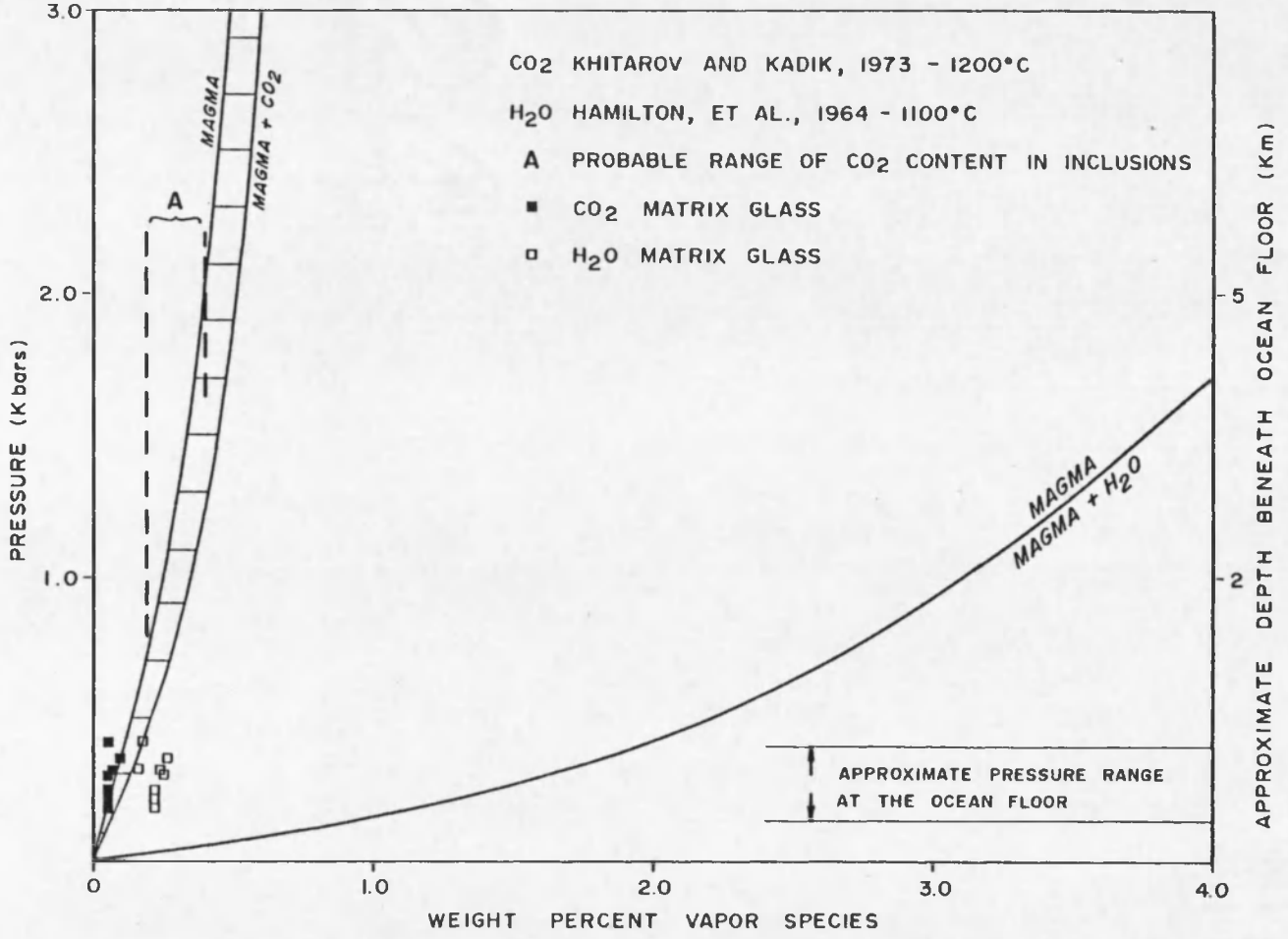

Figure 12. Saturation Curves for Individual Volatile Species in Basaltic Magma.

As demonstrated by Moore (1965, 1970), the H_2O content in sea-floor basalts is distinctly below the solubility limit at the depths of quenching. However, it appears that the CO_2 concentrations of the matrix glasses approximate or are slightly less than the solubility limit for pressures at the ocean floor. If the sum of the partial pressures of all other species made up the difference between P_{CO_2} and P_{TOTAL}, then CO_2 would be the gas dominantly responsible for the matrix glass vesicles. Moore's (1965) data for gases in Hawaiian basalts were used by Anderson (1975) to compute the gas-phase composition in the vesicles of those basalts (see Introduction). Anderson (1975) inferred that CO_2 was rather strongly undersaturated in those basalts (P_{CO_2} = 50 atm at a total pressure of about 470 atm). This assumption was based upon the apparently low CO_2 content of the basaltic glass in Moore's (1965) analyses (CO_2 = 0.01 wt %). The low value for CO_2 combined with similarly low or indeterminate partial pressures of other major gases H_2O, SO_2, H_2S, lead Anderson (1975, p. 47) to state that "The origin of vesicles in deep sea basalts is somewhat uncertain because the sum of the expected partial pressures of the gases is difficult to establish." For the matrix glasses in this study, the CO_2 content is relatively close to the solubility curve which unfortunately has considerable uncertainty in the pressure range of interest. This may mean that the partial pressure of CO_2 was close to the confining pressure. For these samples, it seems reasonable to propose that CO_2 was the dominant volatile species controlling vesiculation. This seems more reasonable in view of the estimates of slightly to distinctly more CO_2 in the inclusions than in the matrix glass. Although the interpretation of this higher CO_2 content is still ambiguous (see

section on Diffusion during Crystal Growth), it is not unreasonable to propose that CO_2-rich vapor has degassed from these basalts in amounts which cannot be readily established. One possible means of evaluating this hypothesis was suggested 12 years ago by Roedder (1965, p. 1775). "A careful search should be made for liquid CO_2 in inclusions in phenocrysts of the tholeiitic basalts, where the possibility of a xenocrystic origin (from nodules) is more remote." A particularly valuable study in terms of the net flux of CO_2 into the surface environment per unit time would be to search glassy rims of sea-floor basalts and oceanic-island basalts for olivine or spinel crystals which had formed deeply enough (15 km?) to sample magma which was saturated with respect to a dense CO_2-rich vapor. The most reasonable samples to search for CO_2-rich inclusions would be the most primitive in terms of high nickel content, low TiO_2, and high Mg/Fe ratio.

An important realization, in regard to an originally higher CO_2 content of M.O.R.B.'s, is that it takes very little time to degas CO_2 from a magma under pressures of 1 to 2 kb. Figure 13 graphically displays calculations based upon a simple Stoke's Law velocity approximation of rising bubbles in a basaltic magma. The density of CO_2 is taken as 0.3 gm/cc (1 kb @ 1200°C) in a magma of density 2.6 gm/cc. Viscosities and bubble sizes cover a broad range which bracket basaltic magma viscosities and vesicle diameters in glassy pillow rims. For example, if the magma viscosity were 10^2 poises, very reasonable for basalt (Shaw, 1972), a bubble with a diameter of 0.1 mm (100μm) would rise 1 km in about 25 years <u>if</u> the magma were not convecting. In fact, magma in a chamber

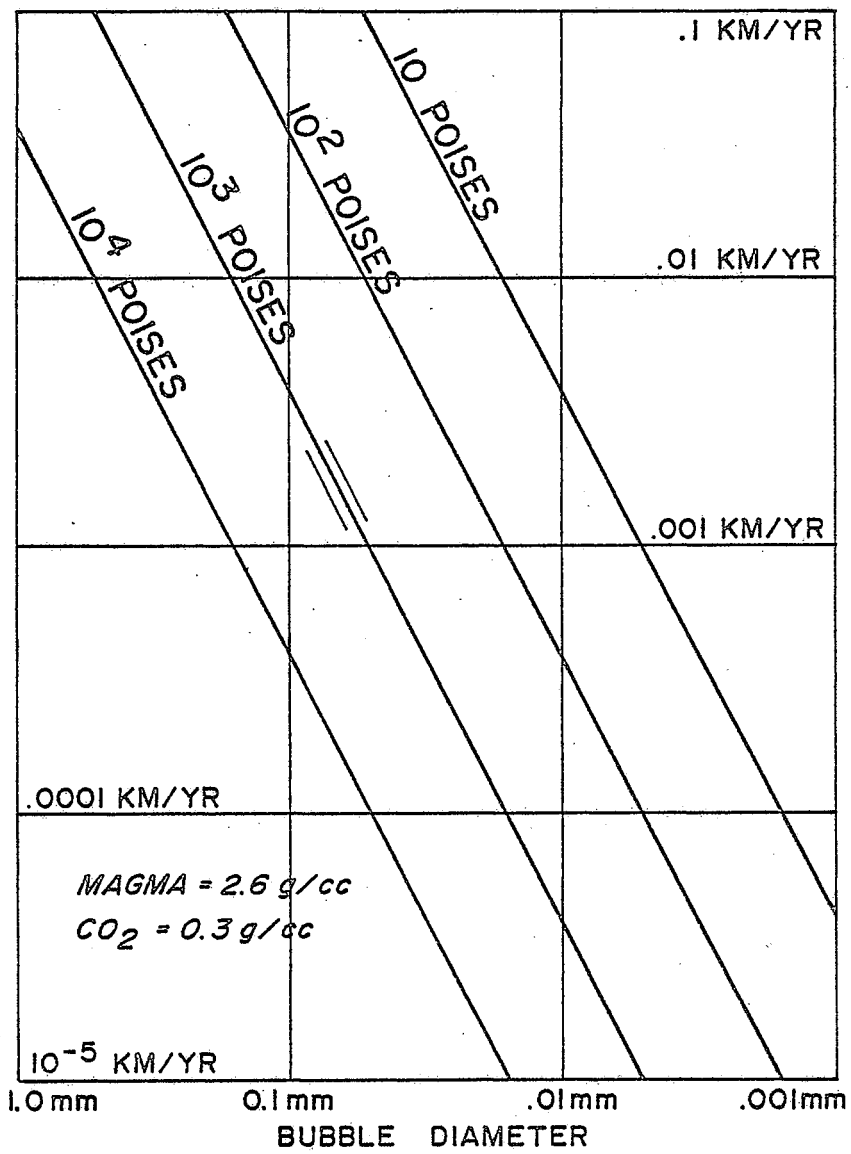

Figure 13. Diagram of Bubble Diameter vs. Stokes Velocity for a CO_2 Bubble Rising through Fluid with Viscosities Ranging from 10 to 10^4 Poises at 1 kbar and 1200°C. -- Most basaltic magmas would fall in the range 10^2 to 10^3. A bubble of 0.1 mm diameter in a magma 10^2 poise would rise 1 km in about 25 years. The velocity is proportional to the bubble radius squared, and because of decompressional effects on solubility and molar volume, rising bubbles would accelerate. A shallow convecting magma chamber beneath a spreading center should be rapidly degassed if sufficient CO_2 were dissolved in the initial magma.

beneath a spreading center would almost certainly be convecting. Many vesicles in glassy rims of pillow basalts on the ocean floor are as much as 1 mm in diameter; had they existed in a deeper magma at 2 to 3 times that pressure, the radius would be reduced by less than 50%. As vapor-saturated magma rises, bubble diameters would be increasing owing to decompressional effects on solubility and molar volume of the vapor. The velocity is a function of the square of the bubble radius, so that bubbles would be accelerating as they rose. The principal point is that a shallow magma chamber beneath a spreading center, such as suggested by Kusznir and Bott (1976), Rosendahl et al. (1976), and Rosendahl (1976), could be rapidly outgassed if the magma originally contained sufficient CO_2. Inclusions which formed prior to entry into such a chamber would record CO_2 and water contents in the shallow subcrustal oceanic mantle.

RAMIFICATIONS OF THE VOLATILE DISTRIBUTION AND ABUNDANCE

Eight out of eight typical tholeiitic basalts from currently active zones of submarine volcanism in the open-ocean basins apparently contained less than 0.01 weight percent water during crystallization of olivine and/or plagioclase phenocrysts. The proposition that the phenocrysts grew from a water-poor magma has an important corollary that the parent magma was at least as water-poor throughout its prior history. This conclusion follows because water is partitioned into a silicate melt in proportion to the total pressure on the system and is not quantitatively degassed while the system remains molten under a significant confining pressure (Khitarov and Kadik, 1973). The olivine tholeiites of this study almost certainly represent partial melts of mantle peridotites. Any available water in the source masses, probably peridotite diapirs, must have been thoroughly scavenged during melting. After segregation of magma from the residual source material, any fractional crystallization which may have occurred would only concentrate volatile components in the remaining liquid. Consequently, the source peridotites for these basalts must have been at least as depleted in water as magma trapped by the inclusions.

Models for generation of basalts under anhydrous conditions have been presented and discussed by Green and Ringwood, 1967; Ito and Kennedy, 1968; O'Hara, 1965, 1968a,b. According to these models olivine and quartz-normative tholeiitic magmas can be produced by partial melting

of peridotites. The models call for either magma segregation from the source peridotite at shallow depths (Green and Ringwood, 1967) or fractional crystallization of olivine at shallow depths (O'Hara, 1968b). In either case, equilibrium between magma and the mineral pair olivine-orthopyroxene under low pressure conditions ensures the nearly silica-saturated character commonly found in many oceanic tholeiites. In discussing a model for basalt genesis based on simplified experimental systems, Kushiro (1969) noted that under anhydrous conditions, the incongruent melting of enstatite terminates at pressures higher than about 5 kb. Because of this effect, Kushiro (1969, p. 161) notes that "silica-saturated magmas can be formed only at pressures below about 6 to 7 kilobars either by partial melting of peridotite or by fractional crystallization of olivine tholeiitic magmas." While all of the basalts in this study are olivine-normative, some are nearly silica-saturated and it seems that a model involving incongruent melting of olivine must be applicable to these rocks, if there are no complications introduced by other volatiles.

Vesicles in the quenched glassy rims of each sample indicate that magmas were saturated with respect to total volatiles at the time of eruption. It is not obvious whether a vapor phase existed throughout the history of the magma or volatile saturation occurred at some unspecified time before quenching. However, it is obvious that if a vapor phase existed throughout the evolution of these magmas, it must have been dominated by carbon and sulfur gases. Subsequent discussion does not treat sulfur as an important petrogenetic variable for two reasons:

1) At this time there is no published data on sulfur solubility or its effects on major silicate phase relationships as a function of pressure in basic magmas, and
2) Sulfur is evidently dissolved in basaltic magmas dominantly as an FeS complex (Haughton, Roeder, and Skinner, 1974; Mathez, 1976), and as such would exert little influence on silicate chemistry and phase relationships.

If sulfur has a minimal effect, then CO_2 is the only other major volatile whose effects must be considered in the petrogenesis of these basalts.

Mysen and Boettcher (1975b) have demonstrated that partial melts of peridotite formed under vapor-present conditions will be critically undersaturated (nepheline normative) if the $CO_2/(CO_2 + H_2O)$ mole ratio is of the order of 0.7 or greater. Their experiments covered the pressure range from 7.5 to 30 kbar, but chemical analyses are reported only on quenched partial melts formed at pressures of 10 kbar or more. The outcome of Mysen and Boettcher's (1975b) experiments seem to be accounted for in terms of the fundamentally different mechanisms by which water and carbon dioxide dissolve in silicate melts (Burnham and Davis, 1971, 1974; Mysen, Eggler, Seitz, and Holloway, 1976). Water is believed to depolymerize a silicate melt by substituting non-bridging hydroxyl radicals for bridging oxygens in Si-O polymers. In contrast, CO_2 apparently dissolves in basic silicate melts as two distinct species, molecular CO_2 and CO_3^{2-} (Mysen et al., 1976). Formation of the latter species in a silicate melt apparently has a polymerizing effect, involving the reaction

$$2(SiO_4)^{4-}(melt) + CO_2\ (vapor) = (Si_2O_7)^{6-}melt + CO_3^{2-}\ (melt).$$

Increased activity of CO_2 in the melt ($a_{CO_2}^{melt}$) drives this reaction to the right producing $(Si_2O_7)^{6-}$ which increases polymerization (Mysen et al., 1976). More polymerized crystalline phases (e.g., enstatite instead of olivine) would precipitate from more polymerized melts. In fact, Eggler (1974) observed a change from an olivine primary phase field to an orthopyroxene primary phase field by essentially saturating an initially volatile-free melt with carbon dioxide in the pressure range 22 to 28 kbars. This observation establishes conclusively that under appropriate conditions, variations in the $a_{CO_2}^{melt}$ alone can exert significant influence on the phase relationships of basic magmas. In other words, all other variables held constant, the more CO_2-rich a peridotite-melt system is, the more stable orthopyroxene is and the more silica-deficient are the partial melts. Precise compositional effects of varying degrees of partial melting are not established by Mysen and Boettcher (1975b), but presumably their conclusions hold for as much as 30% partial melting provided vapor saturation obtains throughout.

The $CO_2/(CO_2 + H_2O)$ mole ratio in the source mass of the basalts in this study must have been very close to 1.0, because of the virtual lack of water. If the basalts are partially melted peridotites formed under vapor-present conditions, they must have:

1) Been extremely silica-deficient initially, assuming they were formed between 10 and 30 kbars, after which they must have experienced extreme fractional crystallization, which is unlikely

in view of the compositional consistency of all samples and the high nickel content of samples 10C1 and 10C4 (for discussion see Ringwood, 1975, p. 160).

2) Formed at pressures lower than 10 kb, and probably lower than 7.5 kbar, such that a pressure-dependent reduction in activity of CO_2 in the melt nullifies the polymerizing effect of the high $CO_2/(CO_2 + H_2O)$ ratio in the source.

The lack of specific data on this low pressure CO_2 effect precludes ruling this option out, although the limited freezing point depression effect (<25°C) of excess CO_2 on a diopside melt system at 7 kb (Rosenhauer and Eggler, 1975) implies that the effects of CO_2 in this range would not be important. The obvious alternative to the vapor-present mode, and the preferred interpretation, is that the magmas formed under vapor-deficient conditions, meaning insufficient volatiles were available to saturate the magma at the depth of segregation from the source mass. Again, this possibility points to a relatively low $a_{CO_2}^{melt}$, implying that an anhydrous model of magma generation accounts for the relationships observed in these basalts. If so, it seems that volatiles did not play an important part in their genesis, and that the depth of magma generation and separation must be relatively shallow (<30 km) (Ringwood, 1975).

Briefly summarizing, if a_S^{melt} is not a significant petrogenetic variable, the virtually anhydrous CO_2-dominant character of the porphyritic basalts in this study restricts the depth of vapor-present partial melting to pressures less than 10 kb or a depth of about 30 km. If there was no vapor phase during most of the partial melting, then the anhydrous

models of Green and Ringwood (1967) and Ringwood (1975) argue cogently for shallow (less than 35 km) partial melting of peridotite to produce at least the nickel-rich, nearly silica-saturated, olivine tholeiites. In either case, shallow melting and magma segregation are indicated for these sea-floor basalts.

These conclusions are compatible with work of previous investigators who have arrived at similar conclusions by quite different lines of reasoning. Kay, Hubbard, and Gast (1970) pointed out the widespread "depleted" nature of sea-floor basalts with regard to trace elements and strontium isotopes. Following the hypothesis of Gast (1968), which calls for at least one previous episode of melting in the source regions for sea-floor basalts, they (Kay et al., 1970) suggested that much of the upper mantle was also depleted in water, and they proposed that most magmas erupting at mid-ocean ridges are the result of shallow melting. Hodges and Bender (1976) have shown that a primitive olivine tholeiite from the FAMOUS area could have been in equilibrium with an olivine and two pyroxenes at about 9 to 10 kbar and they comment (p. 920) that "This multiple phase saturation is consistent with separation of the basaltic liquid from a clinopyroxene bearing residuum at depths of $\sim$30 km beneath the Mid-Atlantic Ridge." DePaolo and Wasserburg (1976a, 1976b) and Richard, Shimazu, and Allegre (1976), using Sm-Nd systematics, confirm at least a two-stage model for the source regions of many oceanic basalts. If basalts in this study are representative of a larger population of tholeiitic basalts from the open-ocean basins, then it is not surprising that major fractions of the sub-oceanic mantle are virtually

anhydrous. One or more previous episodes of partial melting could have effectively withdrawn all water from the source material while leaving behind some of the original carbon dioxide, perhaps as carbonate or as fluid inclusions in solid phases, since CO_2 is much less soluble than water in a silicate melt at comparable pressures (Mysen, 1976; Holloway and Eggler, 1976).

If magmas in this study are found to be representative of oceanic volcanism in general, several additional points may follow logically. First, apparently much less "juvenile" water is being transferred to the surface environment from the mantle per unit time by the single most voluminous type of volcanism on earth than was previously assumed (cf. Anderson, 1975). This suggests that Rubey's (1951) hypothesis of continual degassing of the earth through geologic time to account for "excess volatiles" may require re-examination. Studies of similar, but older assemblages (e.g., ophiolite complexes, Deep-Sea Drilling Project samples) may provide insight into the length of time this condition has existed. Second, either the low-velocity zone requires far less water than is generally proposed (0.1%, Ringwood, 1975) to induce partial melting, or it is not caused by incipient hydrous melting. This point is, of course, quite tentative, but if there is truly no water in many of the magmas leaving the oceanic mantle, then alternative models for the low-velocity zone will have to be sought (e.g., Eggler, 1976). And finally, the initially water-poor nature of the same Mid-Ocean Ridge basalts must constrain access of surface water to the upper mantle beneath spreading centers.

The contrast between the water-poor glass-vapor inclusions and the water-bearing matrix glass seems to require that practically all of the water present in the matrix glass enter the magma after inclusion entrapment. Several objections exist to this hypothetical influx of H_2O into the magma:

1) Matrix glasses which have been analyzed in other studies (Friedman cited in Moore, 1970, p. 276; Craig and Lupton, 1976) give values of δD ($= \frac{(D/H)_{sample} - (D/H)_{standard}}{(D/H)_{standard}} \times 1000$) which are about -50 to -80‰. These values are quite different from Standard Mean Ocean Water (SMOW) for which $\delta D = 0.0‰$, and apparently preclude direct influx of unfractionated seawater into the melt at the ocean floor, because an initially anhydrous melt would instantly take on the hydrogen isotopic "signature" of whatever water enters the magma. Furthermore, the δD value of -50 to -80‰ matches values for phlogopites from peridotite nodules in kimberlites (Sheppard and Epstein, 1970) which almost certainly were derived from the mantle. This range of D/H values has classically been linked with $\delta^{18}O$ values between +2 to +8‰ and labeled "magmatic water", although Taylor (1974) cautions against uncritical usage of such a term. Wenner and Taylor (1973) have shown that some hydroxyl minerals from oceanic crustal rocks have δD values in the range -25 to about -70‰. Should blocks of hydrothermally metamorphosed oceanic crust-bearing amphiboles or antigorite with δD values similar to those bound by Wenner and Taylor (1973) be assimilated by a basaltic magma beneath a spreading

center, the magma would rapidly take on the hydrogen isotopic character of the water-bearing minerals. At this time too little is known about the details of magma-host rock interaction in and around a shallow sub-oceanic magma chamber to rule out such a possibility.

2) The second objection is that $^{3}He/^{4}He$ ratios in the matrix glasses of many pillow basalt rims in other studies (Lupton and Craig, 1976a,b) are much higher than atmospheric values and are interpreted to be primordial (mantle derived). However, the influx of small amounts of water (0.01 mole = 0.2 wt %), particularly if it came from hydroxyl minerals, would probably not introduce sufficient He to modify the ratio. That is, it seems possible to have "crustal" water and "mantle" helium in the same glass.

3) Diffusion of water in static silicate melts is slow and self-arresting (Burnham, 1967) and entry of significant amounts of water at a shallow level into a magma is generally considered unlikely. However, Shaw (1974) demonstrated that a dynamic convecting magma could incorporate and homogenize modest amounts of water under special conditions. It is highly unlikely that a low-viscosity basaltic magma, in a shallow sub-oceanic crustal environment with a high thermal gradient, which probably produces layered gabbros commonly observed in opholite complexes, would be static. Therefore, diffusional arguments against water influx and/or homogenization are not considered serious.

Clearly, the precise location or mechanism by which water might enter the magma cannot be established with data available, but assimilation of previously solidified, hydrothermally metamorphosed blocks of oceanic crust appears to be a reasonable working hypothesis. The principal new component added to the magma could be water, as the bulk chemistry of such blocks should be very similar to the magma. The apparent influx of water at some time after inclusion formation raises an important point. The absence of water in a set of glass-vapor inclusions within phenocrysts places a much more powerful constraint on the source material than does the presence of water. In other words, depending upon the "plumbing" of the volcanic system and the local patterns of crustal (or mantle) water circulation, non-cognate water may enter the magma before phenocryst formation. This water could later be incorporated in the inclusions. Consequently, the presence of water in inclusions of the Marianas sample permits, but does not require, involvement of H_2O in the genesis of those basalts.

Furthermore, as noted by Anderson (1975), H_2O probably is the dominant gas released when a volcano erupts at the surface. But at least in part, this may reflect the fact that every magma which erupts at the earth's surface passes through the hydrous crust of the earth. Had the samples studied in this work erupted at the surface, water would have been the dominant volatile lost. Yet these magmas were once anhydrous. Apparently a hard look must be taken at what is assumed when a "magmatic water" label is assigned on the basis of δD values. A dynamic, severely H_2O-undersaturated magma will almost certainly incorporate some water

upon moving upward in the crust, and it is possible that there are no igneous rocks reaching the earth's surface which have not been at least partly contaminated with water after separation from their source material.

The implications of this study as regards current concepts of basaltic magmatic gases will hinge partly upon the degree to which these samples may be considered representative of a significant volume of volcanic activity. However, it seems likely that much of the water collected in gas analyses from erupting volcanoes was not originally dissolved in the melt. Moreover, the possibility exists that significantly more CO_2 was dissolved in the magmas now erupting along zones of current volcanism, although in view of Mysen and Boettcher's (1975b) work, the nearly silica-saturated nature of many of these rocks may constrain the maximum amount of CO_2 which could originally have been dissolved in the magma. The sulfur content of magmas seems well explained in terms of its iron sulfide solubility, although its pressure-dependent behavior in silicate melts is unexplored experimentally. It seems, therefore, that basaltic magmatic gases of the C-O-H-S system are probably much poorer in water, possibly richer in CO_2, and not much different in terms of sulfur gases than has been suggested by previous workers (see Introduction).

It is noteworthy that the dominant controlling parameter on the amounts of each major gas species dissolved in oceanic tholeiitic basalts is different. These controls may be largely independent until the initiation of wholesale degassing at depths of about 1 km or less (Moore and Schilling, 1973). As noted earlier Haughton et al. (1974) and Mathez

(1976) have demonstrated an important sulfide solubility control on sulfur in many basic magmas. The dominant control on CO_2 content of a melt and vesiculation of the magma may well be solubility of CO_2 gas in the melt, in spite of Anderson's (1975) inference that this does not seem so (Figure 12, see discussion). Solubility clearly has no limiting effect on the amount of water in the basalts quenched below 1 km, and the abundance of water may reflect the length of time available for contamination during the history of the melt. No indication of a relationship between degree of fractionation (e.g., Ni content or Mg/Fe ratio) was found in the limited number samples in this study. However, it is interesting to note that one of the most primitive samples of MORB currently known from the FAMOUS area (527-1-1) contains about 0.08 wt % water (Hodges and Bender, 1976; F. Hodges, personal communication, 1977). If differentiation of MOR basalts takes place in a crustal, sub-oceanic magma chamber, this would provide an ideal site for influx of water, and there may be a correlation between degree of differentiation and water content if enough samples are considered to establish a statistical relationship.

Summary and Conclusions

Glass-vapor inclusions quenched within phenocrysts in the glassy rims of eight submarine tholeiitic pillow basalts from a variety of locations in the open oceans contain less than 0.01 wt % H_2O, about 0.2 to 0.4 wt % CO_2, and about 0.1 wt % S. The enclosing vesiculated matrix glasses contain about 0.2 wt % H_2O, 0.04 to 0.1 wt % CO_2, and about the same amount of sulfur as the inclusions. One tholeiitic basalt sample

from the Marianas Interarc Basin contains inclusions with abundant water, in contrast to otherwise identical inclusions from open-ocean basins.

The glass-vapor inclusions in the samples from the open-ocean basins strongly resemble major and minor (TiO_2, sulfur) elements of the matrix glass, the principal differences being a depletion in the inclusion glass of components which have entered the host phenocryst. These data indicate that the inclusions are samples of matrix magma at an earlier stage in its history. The slight enrichment of CO_2 in the inclusions may reflect either a previously higher CO_2 content in the magma or diffusional accumulation of a rejected component at the crystal-magma interface during crystal growth which was rapid compared to diffusion away from the interface. The water-poor character of the inclusions cannot be accounted for by slow diffusion during crystal growth nor post-entrapment diffusion of water or hydrogen out of the inclusions through the host mineral to the matrix magma. Evidently, the magma was nearly anhydrous when the inclusions were formed. Although the depth of inclusion entrapment is now known, the consistent occurrence of dry inclusions strongly implies that the peridotite source diapirs for each of these basalts were equally dry. The presence of water in the enclosing matrix glass seems to require influx of water into the magma after inclusion entrapment and before quenching. Consequently, the absence of water in inclusions places much more severe constraints upon the source than does the presence of water in inclusions (e.g., Marianas sample). The data indicate that either an anhydrous or very shallow, vapor-present genetic model for the basalts must apply to these samples.

If the basalts in this study represent a much larger population of oceanic tholeiitic basalts erupting along spreading centers and at oceanic islands, then very little water is currently being transferred from the mentle to crustal environments by one of the most voluminous magma types on earth. Estimates of juvenile water input to the surface reservoir may therefore require revision. Incipient hydrous melting as an explanation for the low-velocity zone may have to be re-evaluated if the anhydrous character of the inclusions is found to be widespread on oceanic islands and at spreading centers. The consistently water-rich character of many volcanic gas collections during active basaltic eruptions may represent recycled crystal water rather than water which has been in the magma from its source. Consequently, a true "uncontaminated" basaltic magmatic gas, at least for the samples in this study, would consist almost totally of carbon and sulfur as major components.

APPENDIX A

WHOLE ROCK ANALYSES OF GLASSY PILLOW RIMS

Atomic Absorption Analyses

Fragments of the pillow rims were removed from the samples and cleaned in the manner described in the main text under Sample Preparation (p. 38). Sample preparation for atomic absorption analyses employed the lithium metaborate fusion technique similar to that described by Medlin, Suhr, and Bodkin (1969). A Perkin-Elmer model 403 atomic absorption spectrophotometer was used in the analyses. The details of the method used are described in exhaustive detail by Fouts (1974). The compilation of replicate analyses of BCR-1 (the U. S. Geological Survey basalt standard) represents data obtained through joint effort and applies to the analyses in this study. It is given in Table V and indicates precision and accuracy of the analyses.

Table V. Replicate Analyses of BCR-1.

	Number of Analyses	Standard Deviation	Mean	Literature Value[1]
SiO_2	14	.315	54.44	54.50
TiO_2	12	.043	2.18	2.20
Al_2O_3	15	.155	13.47	13.61
Fe_2O_3-T	15	.133	13.38	13.40
MnO	4	.008	0.18	0.18
MgO	13	.037	3.51	3.46
CaO	14	.197	6.98	6.92
Na_2O	14	.051	3.28	3.27
K_2O	13	.030	1.69	1.70

[1]Flanagan (1973).

Ferrous Iron Analyses

The technique of determining ferrous iron content of the glassy rims of the pillow basalts employed the standard wet-chemical analysis involving titration of an acid digestion solution with a standardized K_2MnO_2 solution. Five replicate analyses of W-1 had a standard deviation of 0.24 about a mean value of 8.60. The preferred value in Flanagan (1973) is 8.72.

APPENDIX B

ELECTRON MICROPROBE ANALYSES OF MATRIX GLASS (MAT) AND INCLUSION GLASS (IG) WITHIN OLIVINE (O) AND PLAGIOCLASE (P) PHENOCRYSTS

	2A-1 (MAT)	2A-1* (MAT)	2A-1 IG1 (0)	2A-1 IG2 (0)	2A-1 IG3 (0)	2A-1 IG4 (0)	2A-1 IG5 (0)	2A-1 IG6 (0)
SiO_2	50.86	(.28)	52.42	52.20	51.61	51.99	52.54	52.28
TiO_2	1.43	(1.22)	1.53	1.55	1.63	1.64	1.76	1.59
Al_2O_3	15.94	(.62)	17.64	16.93	16.81	16.71	17.77	17.28
Cr_2O_3	.05	---	.06	.05	.06	.06	.05	.06
FeO	9.13	(1.03)	8.55	8.95	9.07	8.93	8.29	8.67
MnO	.17	(3.97)	.16	.18	.19	.17	.16	.17
MgO	8.26	(.75)	3.79	4.26	4.55	5.00	3.23	3.92
CaO	11.27	(.44)	12.85	12.96	12.91	12.54	13.15	13.11
Na_2O	2.60	(3.31)	2.67	2.58	2.08	2.68	2.47	2.64
K_2O	.12	(1.96)	.11	.11	.11	.12	.12	.11
P_2O_5	.14	(1.95)	.14	.14	.14	.17	.16	.15
S	.11	(2.84)	.12	.12	.12	.11	.12	.12
NiO	.02	(27.63)	.02	.01	.02	.01	.01	.03
TOTAL	100.10		100.06	100.04	99.30	100.13	99.83	100.13
Mg/Fe (mole ratio)	1.60		.79	.85	.89	.99	.69	.81

	4C1 (MAT)	4C1 G1 (P)	4C1 G2 (P)	4C1 G3 (O)	4C1 G4 (O)	6A4 (MAT)	6A4 G1 (O)	6A4 G2 (O)	6A4 G3 (O)
SiO_2	50.86	51.15	50.82	51.29	51.62	50.82	51.22	50.74	50.96
TiO_2	1.86	.105	1.90	1.94	1.94	1.66	1.78	1.68	1.68
Al_2O_3	14.76	15.11	14.74	15.66	15.66	14.90	15.60	15.10	15.66
Cr_2O_3	.03	.07	.02	.04	.04	.04	.04	.04	.05
FeO	10.46	8.25	10.55	10.10	10.10	9.97	10.08	10.19	10.16
MnO	.19	.18	.21	.18	.18	.18	.19	.18	.19
MgO	7.14	9.97	7.39	4.62	4.62	7.99	4.77	6.69	5.54
CaO	10.78	10.72	10.61	11.74	11.74	10.61	12.02	11.30	12.01
Na_2O	3.05	2.73	2.74	3.05	3.05	3.01	2.87	2.82	2.85
K_2O	.o0	.06	.09	.10	.10	.13	.12	.12	.12
P_2O_5	.16	.07	.16	.17	.17	.15	.17	.17	.17
S	.13	.11	.13	.14	.14	.12	.12	.12	.12
NiO	.02	.01	.02	.02	.02	.01	.02	.01	.01
TOTAL	99.54	99.48	99.38	99.38	99.38	99.59	99.00	99.16	99.52
Mg/Fe (mole ratio)	1.22	2.15	1.25	.81	.81	1.43	.84	1.17	.97

	10C1 (MAT)	10C1 IG1 (O)	10C1 IG2 (O)	10C1 IG3 (O)	10C1 IG4 (O)	10C1 IG5 (P)	10C1 IG6 (P)	10C1 IG7 (P)
SiO_2	47.88	50.05	50.59	49.31	49.19	50.05	49.88	49.38
TiO_2	1.03	1.11	1.24	1.09	.81	.57	.62	.78
Al_2O_3	(17.70)	15.69	16.58	17.77	15.41	17.02	16.94	16.99
Cr_2O_3	.06	.07	.08	.05	---	---	---	---
FeO	8.98	9.25	8.61	9.34	9.11	8.35	8.32	8.48
MnO	.16	.18	.17	.18	.19	.16	.16	.18
MgO	9.20	7.91	5.14	6.02	8.15	8.27	8.21	8.23
CaO	11.10	12.80	13.38	12.90	11.52	11.46	11.41	11.43
Na_2O	2.66	2.33	2.61	2.64	2.47	3.00	2.98	2.87
K_2O	.11	.06	.06	.08	.05	.05	.05	.05
P_2O_5	.08	.08	.08	.11	.13	.05	.06	.11
S	.10	.11	.12	.10	.12	.108	.112	.116
NiO	.05	.02	.01	.02	---	---	---	---
TOTAL	99.11	99.66	98.67	99.61	97.16	99.25	98.85	98.50
Mg/Fe (mole ratio)	1.75	1.53	1.06	1.09	1.59	1.76	1.76	1.73

	10C1 IG8 (P)	10C1 IG9 (P)	10C1 IG10 (P)	10C1 IG11 (P)	10C1 IG12 (P)	R1-24 (MAT)	R1-24 IG1 (P)
SiO_2	48.83	49.73	49.52	49.58	49.78	51.18	51.25
TiO_2	.82	.87	.87	.93	.87	.81	.81
Al_2O_3	17.32	16.86	17.52	16.99	17.34	14.68	14.49
Cr_2O_3	---	---	---	---	---	.03	.03
FeO	8.50	8.59	8.56	8.54	8.65	9.42	9.47
MnO	.16	.15	.16	.15	.16	.19	.17
MgO	8.20	8.04	8.02	8.10	7.99	8.53	8.80
CaO	11.39	11.19	11.32	11.30	11.13	13.31	13.27
Na_2O	2.87	2.93	2.97	2.91	2.90	1.78	1.76
K_2O	.05	.05	.05	.05	.05	.06	.06
P_2O_5	.08	.08	.09	.08	.09	.06	.06
S	.112	.116	.108	.112	.116	.11	.11
NiO	---	---	---	---	---	.01	.00
TOTAL	98.98	98.78	98.87	98.90	99.24	100.17	100.28
Mg/Fe (mole ratio)	1.72	1.67	1.67	1.69	1.65	1.62	1.66

	R1-24 IG2 (P)	R1-24 IG3 (P)	R1-24 IG4 (P)	R1-24 IG5 (P)	R1-24 IG6 (P)	R1-24 IG7 (P)	R1-24 IG8 (P)
SiO_2	50.39	51.44	51.02	51.04	50.90	52.56	52.14
TiO_2	.80	.77	.79	.96	.75	.61	.63
Al_2O_3	14.65	14.73	14.68	14.52	14.57	14.41	14.69
Cr_2O_3	.03	.03	.03	.04	.02	.03	.03
FeO	9.48	8.42	8.48	8.64	9.39	7.81	7.89
MnO	.18	.17	.o7	.17	.20	.15	.14
MgO	8.99	9.32	9.43	9.45	8.89	9.08	9.08
CaO	13.13	13.51	13.33	13.43	13.36	13.41	13.35
Na_2O	1.76	1.74	1.72	1.71	1.80	1.89	1.91
K_2O	.06	.06	.06	.07	.06	.06	.06
P_2O_5	.06	.05	.06	.07	.07	.05	.04
S	.12	.11	.11	.11	.12	.08	.08
NiO	.00	.00	.00	.00	.02	.00	.00
TOTAL	99.65	100.35	99.88	100.21	100.15	100.14	100.04
Mg/Fe (mole ratio)	1.69	1.97	1.98	1.95	1.69	2.07	2.05

	R1-24 IG9 (P)	R1-24 IG10 (P)	R1-24 IG11 (P)	R1-24 IG12 (P)	R1-24 IG13 (P)	R1-8 (MAT)	R1-8 G1 (0)
SiO_2	52.53	51.96	51.99	52.34	51.98	48.30	48.13
TiO_2	.70	.61	.62	8	.56	1.15	1.14
Al_2O_3	13.67	14.36	14.38	14.65	14.03	17.24	17.44
Cr_2O_3	.04	.03	.05	.04	.05	.05	.05
FeO	8.63	8.85	8.51	7.98	8.82	9.77	9.63
MnO	.15	.19	.17	.16	.19	.19	.19
MgO	9.94	9.21	9.42	9.39	9.44	9.52	8.73
CaO	13.23	12.91	13.21	13.06	13.15	11.77	12.02
Na_2O	1.69	1.83	1.81	1.81	.79	2.54	2.50
K_2O	.07	.07	.07	.07	.07	.05	.06
P_2O_5	.05	.04	.04	.03	.03	.06	.06
S	.09	.09	.09	.07	.08	.12	.13
NiO	.00	.00	.00	.01	.03	.01	.02
TOTAL	100.79	100.15	100.36	100.09	99.22	100.77	100.10
Mg/Fe (mole ratio)	2.05	1.86	1.97	2.10	1.91	.97	.91

	R1-8 G2 (0)	R1-8 G3 (0)	R1-8 G4 (0)	R1-8 G5 (0)	R1-8 G6 (0)	R1-8 G7 (0)	R1-8 G8 (0)	R1-8 G9 (0)
SiO_2	49.83	47.78	48.73	48.64	48.92	47.73	48.65	48.91
TiO_2	1.19	1.19	1.24	1.16	1.13	1.15	1.10	1.14
Al_2O_3	19.67	18.01	18.14	17.60	17.37	17.12	17.56	17.83
Cr_2O_3	.06	.05	.05	.03	.05	.04	.04	.06
FeO	8.48	9.60	8.85	9.66	9.64	10.13	10.13	9.61
MnO	.19	.16	.17	.18	.17	.16	.19	.16
MgO	5.27	8.06	7.87	8.91	8.89	8.61	8.06	7.35
CaO	12.22	12.66	12.44	11.79	11.97	12.16	12.48	12.75
Na_2O	2.46	2.46	2.87	2.56	2.59	2.43	2.39	2.54
K_2O	.05	.05	.05	.05	.05	.05	.05	.05
P_2O_5	.06	.06	.05	.07	.06	.07	.06	.07
S	.13	.12	.12	.13	.13	.13	.13	.14
NiO	.02	.02	.04	.01	.01	.02	.02	.02
TOTAL	99.63	100.22	100.62	100.79	100.98	99.80	100.86	100.63
Mg/Fe (mole ratio)	.62	.84	.89	.92	.92	.85	.80	.76

	R1-10 (MAT)	R1-10 G1 (0)	R1-10 G2 (0)	R1-10 G3 (0)	R1-10 G4 (0)	46D10 (MAT)	46D10 G1	46D10 G2
SiO_2	50.o0	49.60	49.86	49.89	49.85	52.30	52.43	51.57
TiO_2	2.33	2.35	2.33	2.26	2.40	1.92	1.99	1.91
Al_2O_3	13.73	13.93	13.79	13.74	13.40	15.68	15.34	15.74
Cr_2O_3	.00	.01	.01	.00	.00	.01	.01	.02
FeO	13.04	12.93	12.88	12.39	12.74	9.53	9.58	9.28
MnO	.23	.23	.23	.21	.23	.19	.19	.19
MgO	5.99	5.88	5.52	6.38	6.06	5.47	5.34	4.53
CaO	10.81	10.76	10.82	11.00	10.85	9.78	9.65	10.03
Na_2O	3.14	3.09	3.10	2.95	3.09	2.87	2.26	2.63
K_2O	.32	.33	.32	.31	.34	.55	.44	.58
P_2O_5	.24	.24	.25	.24	.25	.29	.32	.30
S	.17	.17	.17	.17	.18	.11	.12	.11
NiO	.00	.00	.00	.01	.01	.01	.01	.00
TOTAL	100.10	99.52	99.28	99.55	99.40	98.71	97.68	96.89
MgO/FeO	.46	.45	.43	.52	.48	.57	.56	.49

	46D10 G3	R1-11 (MAT)	R1-11 G1 (0)	R1-11 G3 (0)	R1-11 G4 (0)	R1-15-1 (MAT)	15-1 G1 (0)
SiO_2	52.74	49.72	50.42	49.77	49.74	49.92	52.63
TiO_2	2.00	1.80	1.91	1.95	1.82	2.59	2.96
Al_2O_3	15.42	13.98	15.56	14.43	14.16	16.42	18.86
Cr_2O_3	.01	.02	.30	.01	.01	.02	.03
FeO	9.76	12.02	10.90	12.03	12.24	9.75	8.38
MnO	.19	.22	.20	.23	.19	.17	.17
MgO	5.60	6.69	3.61	4.83	5.74	6.94	2.61
CaO	9.79	11.48	13.53	12.62	12.55	9.35	9.88
Na_2O	2.70	3.00	2.94	3.01	2.88	2.99	2.25
K_2O	.56	.24	.24	.28	.22	1.09	.92
P_2O_5	.29	.17	.17	.19	.17	.54	.60
S	.12	.17	.17	.18	.18	.12	.14
NiO	.01	.02	.01	.02	.00	.00	.00
TOTAL	99.19	99.53	99.96	99.55	99.90	99.90	99.43
FeO/MgO						1.40	3.21
MgO/FeO	.57	.56	.33	.40	.46	.71	.31

	15-1 G2 (0)	15-1 G3 (0)	15-1 G4 (0)	15-1 G5 (0)	R1-18-2 (MAT)	18-2 G1 (0)	18-2 G2 (0)	18-2 G3 (0)
SiO_2	50.03	50.78	49.65	51.17	48.40	48.80	48.32	49.29
TiO_2	2.73	2.87	2.74	2.74	1.56	1.72	1.56	1.54
Al_2O_3	17.04	17.58	16.84	17.27	17.15	17.43	17.39	18.56
Cr_2O_3	.04	.02	.03	.03	.03	.03	.04	.04
FeO	9.82	9.51	10.01	9.36	9.60	9.43	9.84	9.02
MnO	.17	.18	.19	.19	.16	.17	.17	.16
MgO	4.41	3.09	4.70	4.14	8.76	8.46	8.07	6.02
CaO	10.59	11.29	10.64	10.73	11.50	11.73	11.89	12.21
Na_2O	2.97	2.52	2.43	2.30	2.89	2.96	2.13	2.92
K_2O	1.03	1.03	1.02	1.07	.09	.09	.09	.08
P_2O_5	.58	.60	.56	.61	.14	.15	.17	.14
S	.13	.14	.13	.14	.13	.14	.13	.13
NiO	.00	.00	.03	.01	.01	.01	.03	.02
TOTAL	99.54	99.61	98.97	99.76	100.42	10o.12	99.83	100.13
FeO/MgO	2.23	3.08	2.13	2.26				
MgO/FeO	.45	.32	.47	.44	.91	.90	.82	.66

	RI-19-2 (MAT)	19-2 G1 (0)	19-2 G2 (0)	19-2 G3 (0)	19-2 G4 (0)
SiO_2	47.99	48.07	48.14	48.66	47.38
TiO_2	1.36	1.38	1.38	1.44	1.45
Al_2O_3	17.55	18.14	17.98	18.16	17.44
Cr_2O_3	.04	.03	.32	.03	.02
FeO	9.99	9.69	9.60	10.13	9.87
MnO	.18	.17	.18	.18	.19
MgO	8.69	8.53	7.78	6.81	8.39
CaO	11.48	11.42	12.19	12.21	10.93
Na_2O	2.80	2.72	2.72	2.77	2.76
K_2O	.17	.17	.16	.17	.17
P_2O_5	.13	.15	.14	.15	.14
S	.13	.12	.13	.13	.13
NiO	.01	.04	.01	.01	.01
TOTAL	100.52	100.63	100.73	100.85	98.88
MgO/FeO	.87	.88	.81	.67	.85

*Relative standard deviation of 10 randomly chosen 30μm diameter spots in clear matrix glass. These values are for 2Al but are typical of all matrix glasses.

APPENDIX C

VOLATILE ANALYSES

The samples for all volatile analyses were prepared in a manner which is similar to that described in the text under the section on Sample Preparation (p. 38) for mass spectrometric analysis. Only clean, virtually crystal-free fragments of matrix glass were analyzed and the values are considered to represent concentrations which existed in the magma at the time of quenching.

Sulfur

During this study sulfur was analyzed using three distinctly different techniques--mass spectrometry, low total-sulfur inducation furnace, and electron microprobe. The results are listed in Table VI. The mass spectrometric method is described in detail by Killingley and Muenow (1975a). They estimate a relative standard deviation of 7% for the technique.

The Leco method is described by Moore et al. (1972) and uses samples ranging up to 100 mg. Analyses were performed using a Leco 532-000 sulfur analyzer. Fusion of the sample above 1400°C in a ceramic crucible with iron chips and a vanadium accelerator is achieved in a flowing oxygen atmosphere producing SO_2. The combustion products are carried to an automatic titration vessel containing dilute HCl, KI, and a starch indicator. Titration with KIO_3 solution with an automatic buret is to a preselected blue end point. A silicate matrix sulfur standard is used

Table VI. Comparison of Sulfur Values for Three Analytical Techniques.

Sample No.	Leco (ppm)	M.S. (ppm)	MICROPROBE Wt %	MICROPROBE Std. Dev.[1]
2A1	1170	1295	.14	1.98
3A3	----	1200	.11	15.77
4C1	1310, 1390	1386, 1470	.14	3.20
6A4	1280, 1390, 1380	974	.12	3.01
7A4	1420	1455		
10C1	970	1700 920	.10	6.73
10C4	1380	1550, 1350		
10C18	1340		.13	3.5
R1-24	1210	1000	.11	4.2

[1]Standard deviation of 10 randomly chosen spot analyses in the matrix glass.

for control of the end point. The precision of the method ranges from about 10% for basalt samples below 50 mg to about 4% for larger samples on the order of 100 mg.

The electron microprobe analyses are described in the body of the text in the section on Sample Description and Analysis (p. 8). The agreement of the three techniques implies an approach to 'truth'. Although the glasses seem quite homogeneous by the criterion of multiple microprobe analyses, there is still the sampling problem of occasionally incorporating a sulfide grain in one of the bulk-type analyses and thereby substantially enhancing the sulfur value in a single analysis.

Water

Water is usually the dominant volatile released from the matrix glass. Standard chemical analyses report H_2O^- as vapor driven off the sample below 110°C or 150°C (see Moore and Schilling, 1973). Water which leaves the sample above this low temperature is assigned to H_2O^+. As demonstrated in Figure 8, the standard method of water analysis does not adequately extract "low temperature" water and may produce values of H_2O^+ which are artificially high. Moore and Schilling (1973) confronted this problem and found that H_2O^{110+} (water released avove 110°C) was commonly 30 to 70% higher than H_2O^{150+}. Reference to Figure 8 indicates why this might have been. Degassing of the crystalline interior of a pillow produces a broad large water peak which reaches a maximum at about 210°C then tapers gradually to a minimum at about 1200 to 1400°C. In contrast, the matrix glasses released water in two well-defined peaks between 700

and 980°C. Notably, the standard methods of water analysis should give good values for water if only pure glass is used. It is this high temperature water which is reported here and the mass spectrometer method is the most effective method of extracting this water.

Killingley and Muenow (1975a) observed similar patterns of water release for submarine basaltic glasses from Hawaii which had initially been studied by Moore (1965). Agreement between Moore's published analyses for H_2O^+ using the Penfield Method and those by Killingley and Muenow (1975a) are within 15% with results of the mass spectrometric method being slightly higher. A detailed comparison is given in Table I of Killingley and Muenow (1975a) for multiple analyses of H_2O.

A gas chromatographic water analysis completed at The University of Arizona and water analyses by mass spectrometric method (similar to Killingley and Muenow, 1975a) are presented in Table VII.

Table VII. Comparison of H_2O Analyses by Mass Spectrometer and Gas Chromatograph.

Sample No.	Wt % (M.S.)	Wt % (G.C.)
2A1	0.23	0.25, 0.20, 0.18
3A3	0.26	0.22, 0.19
4C1	0.23, 0.29	0.16
6A4	0.19	0.13
7A4	0.26	0.28, 0.20
10C1	0.34, 0.24	0.21
10C4	0.21, 0.20	0.27
10C18	--	0.18

The gas chromatographic method employed a Hewlett-Packard 9100A Research Gas Chromatograph with a cryogenic capability. A thermal conductivity detector and dual 12 ft, ¼ in columns of Poropak 'Q' were employed for water and CO_2 analyses. One gram samples of pure glass were heated in a static originally evacuated system to about 1250°C. The evolved gases were collected in a calibrated volume glass bulb in which pressure was monitored using a tiny integrated circuit pressure transducer made by National Semi-Conductor Corporation. The bulb was maintained at a constant temperature; pressures never exceeded 150 mm Hg. The total number of moles of gas collected was calculated using the ideal gas law. Aliquots of the gas were then injected into the chromatographic column. Percentages of gas aliquots were applied to the total number of moles of gas calculated to give the amount of each gas evolved. The method did not work well for SO_2 and H_2S and sulfur was quantitatively removed before the collection bulb. The dominant gases were CO_2 and H_2O with minor N_2 (<1.0%). The system was standardized using known mixtures of CO_2 and H_2O. Adequate sample standards were not found and the accuracy is not well known. The precision is estimated at $\pm$ 20% for both gases; H_2O values are believed to be low due to differential adsorption on walls of tubing, which would produce CO_2 values which are equally high.

The mass spectrometer values for water are considered to be superior to those by gas chromatograph and these are the numbers presented in Table IV.

Carbon Dioxide

For determination of total carbon, samples were burned in a flowing oxygen atmosphere to form CO_2. Following purification and trapping stages of the effluent gases, CO_2 is detected using a Leco 589-400 gas chromatographic low-carbon analyzer. A differential thermal conductivity detector was utilized. National Bureau of Standards low-carbon steel (101e) was used to construct standard and analytical curves. The combustion-gas chromatographic detection technique cannot distinguish the chemical state of carbon in the sample. The precision of each analysis is taken from the 90 percent confidence level on the regression line for the reference standards and is always less than $\pm$ 10% of the value quoted (Moore et al., 1971).

Carbon values from the gas chromatographic technique described under Water Analyses generally agreed with the values from Leco analyses. However, the CO_2 values determined on matrix glasses by the mass spectrometric method were consistently higher, by a factor of 2 to 3, than the Leco values. The discrepancy has not yet been resolved between the two methods. Values for the Leco analyses are considered to be more accurate at this time, by this author, because of the less complicated correction procedures and fewer problems of interference. The CO_2/H_2O values computed in the pyrogram (Figure 7; Table IV) for matrix glasses have used Leco carbon values. Differences of 2 to 3 times between the values for CO_2 in the matrix glass do not seriously affect the interpretation because 1) the lower of the two values has been chosen to base

interpretations on and higher values would make several of the interpretive points stronger (e.g., saturation of the magma, p. 73), 2) the difference in CO_2/H_2O ratios for matrix glass ($\sim$0.1/1.0) and inclusions (>30/1) is so large that relatively small changes in the absolute amount of CO_2 will not significantly influence the difference.

REFERENCES

Anderson, A. T., 1974, Before eruption H_2O content of some high alumina magmas: Bull. Volcanol., v. 37, p. 530-552.

_____, 1975, Some basaltic and andesitic gases: Rev. Geophys. Space Phys., v. 13, p. 37-56.

Anderson, A. T., and Wright, T. L., 1972, Phenocrysts and glass inclusions and their bearing on oxidation and mixing of basaltic magmas, Kilauea Volcano, Hawaii: Am. Mineral., v. 57, p. 188-216. 216.

Arnason, B., and Sigurgeirsson, T., 1968, Deuterium content of water vapor and hydrogen in volcanic gas at Surtsey: Geochim. Cosmochim. Acta, v. 32, p. 807-813.

Bazarova, T. Y., Canilho, E. M., Sobolev, V. S., and Shugorova, N. A., 1973, Temperature and conditions of crystallization of alkaline effusives from the Majo Isle (Cape Verde): Lithos 6, p. 403-411.

Bottinga, Y., and Weill, D. F., 1970, Densities of liquid silicate systems calculated from partial molar volumes of oxide components: Am. Jour. Sci., v. 269, p. 169-182.

Burnham, C. W., 1967, Geochemistry of hydrothermal ore deposits, H. L. Barnes (ed.), Holt, Rinehart, and Winston, New York, p. 34-76.

Burnham, C. W., and Davis, N. F., 1971, The role of H_2O in silicate melts, I, P-V-T relations in the system $NaAlSi_3O_8$-H_2O to 10 kilobars and 1000°C: Amer. Jour. Sci., v. 270, p. 54-79.

_____, 1974, The role of H_2O in silicate melts; II, Thermodynamic and phase relations in the system $NaAlSi_3O_8$-H_2O to 10 kilobars, 700° to 1100°C: Am. Jour. Sci., v. 274, p. 902-940.

Chamberlain, R. T., 1908, The gases in rocks: Carnegie Inst. Wash. Pub. 106, p. 1-80.

Craig, H., and Lupton, J. E., 1976, Rare gases and volatiles in oceanic basalts (Abst.): E.O.S., Trans. Am. Geophys. Union, v. 57, p. 408.

DePaolo, D. J., and Wasserburg, G. J., 1976a, Inferences about magma sources and mantle structure from variations of $^{143}Nd/^{144}Nd$: Geophys. Res. Lett., v. 3, no. 2, p. 743-746.

_____, 1976b, Nd isotopic variations of petrogenetic models: Geophys. Res. Lett., v. 3, p. 744-752.

Drake, M. J., 1976, Plagioclase-melt equilibria: Geochim. Cosmochim. Acta, v. 40, p. 457-465.

Dymond, J., and Hogan, L., 1973, Noble gas abundance patterns in deep-sea basalts - primordial gases from the mantle: Earth Planet. Sci. Lett., v. 20, p. 131-139.

Eggler, D. H., 1974, Effect of CO_2 on the melting of peridotite: Carnegie Inst. Wash., Yearbook 1973, p. 215-224.

_____, 1975, CO_2 as a volatile component in the mantle: The system Mg_2SiO_4-SiO_2-H_2O-CO_2: Phys. Chem. Earth, v. 9, p. 869-881.

_____, 1976, Does CO_2 cause partial melting in the low-velocity layer of the mantle?: Geology, v. 4, p. 69-72.

Finlayson, J. B., Barnes, I. L., and Naughton, J. J., 1968, Developments in volcanic gas research in Hawaii in the crust and upper mantle of the Pacific area: Geophys. Monogr. Ser., v. 12, L. Knopoff, C. L. Drake, and P. J. Hart (eds.), A.G.U., Washington, D. C., p. 428.

Flanagan, F. J., 1973, 1972 values for international geochemical reference samples: Geochim. Cosmochim. Acta, v. 137, p. 1189-1200.

Fouts, J. A., 1974, Petrology and chemistry of some diabase sills in central Arizona: Ph.D. Dissertation, The University of Arizona, 158 p.

Frey, F. A., Bryan, W. B., and Thompson, G., 1974, Atlantic Ocean floor geochemistry and petrology of basalts from legs 2 and 3 of the Deep-Sea Drilling Project: Jour. Geophys. Res., v. 79, p. 5507-5527.

Gast, P. W., 1968, Trace element fractionation and the origin of tholeiitic and alkaline magma types: Geochim. Cosmochim. Acta, v. 32, p. 1057-1086.

Gerlach, T. M., and Nordlie, B. E., 1975, Part I. Composition limits and trends in basaltic glasses: Am. Jour. Sci., v. 275, p. 353-376.

Green, D. H., and Ringwood, A. E., 1967, An experimental investigation of the gabbro to eclogite transformation and its petrological applications: Geochim. Cosmochim. Acta, v. 31, p. 767-833.

Grimley, R. T., 1967, Mass spectrometry, in The Characterization of High Temperature Vapors, J. L. Margrave (ed.), John Wiley and Sons, New York, p. 195-243.

Hamilton, D. C., Burnham, C. W., and Oxborn, E. F., 1964, The solubility of water and effects of oxygen fugacity and water content on crystallization in mafic magmas: Jour. Petrol., v. 5, p. 21-39.

Haughton, D. R., Roeder, P. L., and Skinner, B. J., 1974, Solubility of sulfur in mafic magmas: Econ. Geol., v. 69, p. 451-467.

Heald, E. F., Naughton, J. J., and Barnes, I. L., Jr., 1963, the chemistry of volcanic gases; 2. Use of equilibrium calculations in the interpretation of volcanic gas samples: Jour. Geophys. Res., v. 68, p. 545-577.

Hodges, F. L., and Bender, J. F., 1976, Petrogenesis of basalt glass from project FAMOUS: Experimental study from 1 atm to 15 kbar (Abst.): Geol. Soc. America Abst. with Programs, v. 8, no. 6, p. 920.

Holloway, Jr., and Burnham, C. W., 1972, Melting relations of basalt with equilibrium water pressure less than total pressure: Jour. Petrol., v. 13, p. 1-29.

Holloway, J. R., and Eggler, D. H., 1976, Fluid-absent melting of peridotite containing phlogopite and dolomite: Carnegie Inst. Wash. Yearbook 1976, p. 636-639.

Ito, K., and Kennedy, G. C., 1968, Melting and phase relations in the plane tholeiite-lherzolite-nepheline basanite to 40 kbar with geological implications: Contrib. Mineral. Petrol., v. 19, p. 177-211.

Iwasaki, I., Ozawa, T., Yoshida, M., Katsura, T., Iwasaki, B., and Kamada, M., 1963, Nature of volcanic gases and volcanic eruption: Bull. Volcanol., v. 26, p. 73-81.

Jaggar, T. A., 1940, Magmatic gases: Am. Jour. Sci., v. 23, no. 5, p. 312-353.

Katsura, T., and Nagashima, S., 1974, Solubility of sulfur in magmas: Geochim. Cosmochim. Acta, v. 3, p. 517-531.

Kay, R., Hubbard, N. J., and Gast, P. W., 1970, Chemical characteristics and origin of oceanic ridge volcanic rocks: Jour. Geophys. Res., v. 75, p. 1585-1613.

Khitarov, N. I., and Kadik, A. A., 1973, Water and carbon dioxide in magmatic melts and peculiarities of the melting process: Contrib. Mineral. Petrol., v. 41, p. 205-215.

Killingley, J. S., and Muenow, D. W., 1974, A mass spectrometric method for the determination of the size distribution of CO_2 inclusions in olivine: Am. Mineralogist, v. 59, p. 863-867.

_____, 1975a, Volatiles from Hawaiian submarine basalts determined by dynamic high temperature mass spectrometry: Geochim. Cosmochim. Acta, v. 39, p. 1467-1473.

_____, 1975b, Thermal stress-induced release of CO_2 inclusions in olivine on cooling from high temperatures: Am. Mineralogist, v. 60, p. 148-151.

Kudo, A. M., and Weill, D. F., 1970, An igneous plagioclase thermometer: Contrib. Mineral. Petrol., v. 25, p. 52-65.

Kushiro, I., 1969, Liquidus relations in the system forsterite-diopside-silica-H_2O: Carnegie Inst. Wash., Yearbook 1967, p. 158-161.

_____, 1972, Effect of water on the composition of magmas formed at high pressures: Jour. Petrol., v. 13, p. 311-334.

Kusznir, N. J., and Bott, M. H. P., 1976, A thermal study of the formation of oceanic crust: Geophys. Jour. Royal Astr. Soc., v. 47, p. 83-95.

Leguern, F., 1972, Etudes dynamiques sur la phase gazeuse eruptive: Rapp. CEA-R-4383, Serv. de Doc., Commis. a l'Energ. At., Gif-sur-Yvette, France, 169 p.

Lupton, J. E., and Craig, H., 1976a, Excess ^3He in oceanic basalts: Evidence for terrestrial primordial helium: Earth Planet. Sci. Lett., v. 26, p. 133-139.

_____, 1976b, Primordial helium in oceanic basalts (Abst.): E.O.S., Trans. Am. Geophys. Union, v. 57, p. 408.

Mathez, E. A., 1973, Refinement of the Kudo-Weill plagioclase thermometer and its application to basaltic rocks: Contrib. Mineral. Petrol., v. 41, p. 61-72.

_____, 1976, Sulfur solubility and magmatic sulfides in submarine basalt glass: Jour. Geophys. Res., v. 81, p. 4269-4276.

Mathez, E. A., and Yeats, R. S., 1976, Magmatic sulfides in basalt glass from DSDP sites 319A and 320, Nazca Plate, in Initial Reports of the Deep-Sea Drilling Project: U. S. Govt. Printing Office, v. 34, Washington, D. C.

Medlin, J. H., Suhr, N. H., and Bodkin, J. B., 1969, Atomic absorption analysis of silicates employing $LiBO_2$ fusions: Atomic Abs. Newsletter, v. 8, p. 25-29.

Moore, C. B., Lewis, C. F., Cripe, J., Delles, F. M., Kelly, W. R., and Gibson, E. K., Jr., 1972, Total carbon, nitrogen, and sulfur in Apollo 14 lunar samples: Proc. 3rd Lunar Science Conf., Geochim. Cosmochim. Acta, Suppl. 3, v. 2, p. 2051-2058.

Moore, C. B., Lewis, C. F., Larimer, J. W., Delles, F. M., Gooley, R., and Nichiporuk, W., 1971, Total carbon and nitrogen abundances in Apollo 12 lunar samples: Proc. 2nd Lunar Sci. Conf., Goechim. Cosmochim. Acta, Suppl. 2, v. 2, p. 1343-1350.

Moore, J. G., 1965, Petrology of deep-sea basalt near Hawaii: Am. Jour. Sci., v. 263, p. 40-52.

_____, 1970, Water content of basalt erupted on the ocean floor: Contrib. Mineral. Petrol., v. 28, p. 272-279.

_____, 1975, Mechanism of formation of pillow lava: American Scientist, v. 63, p. 269-277.

Moore, J. G., and Calk, L., 1971, Sulfide spherules in vesicles of dredged pillow basalt: Am. Mineralogist, v. 56, p. 476-488.

Moore, J. G., and Fabbi, B, P., 1971, An estimate of the juvenile sulfur content of basalt: Contrib. Mineral. Petrol., v. 33, p. 118-127.

Moore, J. G., and Schilling, J. G., 1973, Vesicles, water and sulfur in Reykjanes Ridge basalts: Contrib. Mineral. Petrol., v. 41, p. 105-118.

Muenow, D. W., 1973, Occurrence of volatile nitrides from silicates in low-pressure high-temperature reducing environments: Geochim. Cosmochim. Acta, v. 37, p. 2523-2528.

Mysen, B. O., 1975, Partitioning of iron and magnesium between crystals and partial melts in peridotite upper mantle: Contrib. Mineral. Petrol., v. 52, p. 69-76.

_____, 1976, The role of volatiles in silicate melts: Solubility of carbon dioxide and water in feldspar, pyroxene, and feldspathoid melts to 30 kb and 1625°C: Am. Jour. Sci., v. 276, p. 969-996.

Mysen, B. O., and Boettcher, A. L., 1975a, Melting in a hydrous mantle: I, Phase relations of natural peridotite at high pressures and temperatures with controlled activities of water, carbon dioxide, and hydrogen: Jour. Petrol., v. 16, p. 520-548.

_____, 1975b, Melting of a hydrous mantle: II, Geochemistry of crystals and liquids formed by anatexis of mantle peridotite at high pressures and high temperatures as a function of controlled activities of water, hydrogen and carbon dioxide: Jour. Petrol., v. 16, p. 549-593.

Mysen, B. O., Eggler, D. H., Seitz, M. G., and Holloway, J. R., 1976, Carbon dioxide in silicate melts and crystals: I, Solubility measurements: Am. Jour. Sci., v. 276, p. 455-479.

Naughton, J. J., Derby, J. V., and Glover, R. B., 1969, Infrared measurements on volcanic gas and fume: Kilauea eruptions, 1968: Jour. Geophys. Res., v. 74, p. 3273-3277.

Naughton, J. J., Heald, E. F., and Barnes, J. L., 1963, The chemistry of volcanic gases: I, Collection and analysis of equilibrium mixtures by gas chromatography: Jour. Geophys. Res., v. 68, p. 538-544.

Nordlie, B. E., 1971, The composition of the magmatic gas of Kilauea and its behavior on the near-surface environment: Am. Jour. Sci., v. 271, p. 417-463.

O'Hara, M. J., 1965, Primary magmas and the origin of basalts: Scott. Jour. Geol., v. 1, p. 19-40.

_____, 1968a, The bearing of phase equilibria studies in synthetic and natural systems on the origin and evolution of basic and ultrabasic rocks: Earth Sci. Rev., v. 4, p. 69-133.

_____, 1968b, Are ocean-floor basalts primary magma?: Nature, v. 220, p. 683-686.

Pearce, T. H., Gorman, B. E., and Birkett, T. C., 1975, The TiO_2-K_2O-P_2O_5 diagram: A method of discrimination between oceanic and non-oceanic basalts: Earth Planet. Sci. Lett., v. 24, p. 419-426.

Pineau, F., Javoy, M., and Bottinga, Y., 1976, $^{13}C/^{12}C$ ratios of rocks and inclusions in popping rocks on the Mid-Atlantic Ridge and their bearing on the problem of the isotopic composition of deep-seated carbon: Earth Planet. Sci. Lett., v. 29, p. 413-421.

Puccetti, A., and Buddemeier, R. W., 1974, Volcanic CO_2 emissions: A ^{14}C study of Kilauea volcano (Abst.): E.O.S., Trans. Am. Geophys. Union, v. 55, no. 4, p. 488.

Richard, P., Shimazu, N., and Allegre, C. J., 1976, $^{143}Nd/^{146}Nd$, a natural tracer: An application to oceanic basalts: Earth Planet. Sci. Lett., v. 31, p. 269-278.

Ringwood, A. E., 1975, Composition and petrology of the earth's mantle: McGraw-Hill, Inc., New York, 618 p.

Roedder, E., 1965, Liquid CO_2 inclusions in olivine-bearing nodules and phenocrysts from basalts: Am. Mineralogist, v. 50, p. 1746-1782.

Roedder, E., and Weiblen, P. W., 1972, Petrographic features and petrologic significance of melt inclusions in Apollo 14 and 15 rocks: Geochim. Cosmochim. Acta, Suppl. 3, Proceedings of the 3rd Lunar Sci. Conf., v. 1, p. 251-279.

_____, 1973a, Petrology of melt inclusions in Apollo samples 15598 and 62295, and of clasts in 67915 and several lunar soils: Geochim. Cosmochim. Acta, Suppl. 4, Proceedings of the 4th Lunar Sci. Conf., v. 1, p. 681-703.

_____, 1973b, Petrology of some lithic fragments from Luna 20: Geochim. Cosmochim. Acta, v. 37, p. 1031-1052.

Roeder, P. L., and Emslie, R. F., 1970, Olivine-liquid equilibrium: Contrib. Mineral. Petrol., v. 29, p. 275-289.

Rosendahl, B. R., 1976, Evolution of oceanic crust: 2, Constraints, implications, and inferences: Jour. Geophys. Res., v. 81, p. 5305-5314.

Rosendahl, B. R., Raitt, R. W., Dorman, L. M., Bibee, L. D., Hussong, D. M., and Sutton, G. H., 1976, Evolution of oceanic crust: 1, A physical model of the East Pacific rise crest derived from seismic refraction data: Jour. Geophys. Res., v. 81, p. 5294-5304.

Rosenhauer, M., and Eggler, D. H., 1975, Solution of H_2O and CO_2 in diopside melt: Carnegie Inst. Wash. Yearbook 1974, p. 474-479.

Rubey, W. W., 1951, Geologic history of sea water: Geol. Soc. America Bull. 62, p. 1111-1148.

Rucklidge, J. C., and Gasparrini, E. L., 1969, EMPADR VII - Electron microprobe analytical data reduction program, version 7: Dept. Geol., University of Toronto.

Shaw, H. R., 1972, Viscosities of magmatic silicate liquids: An empirical method of prediction: Am. Jour. Sci., v. 272, p. 870-893.

Shaw, H. R., 1974, Diffusion of H_2O in granitic liquids: Part I, experimental data; Part II, mass transfer in magma chambers, in A. W. Hoffman, B. J. Giletti, H. S. Yoder, Jr., and R. A. Yund (eds.), Geochemical Transport and Kinetics, Carnegie Inst. Wash. Pub. 634, p. 139-170.

Shepherd, E. S., 1938, The gases in rocks and some related problems: Am. Jour. Sci., v. 35A, p. 311-351.

Sheppard, S. M., and Epstein, S., 1970, D/H and $^{18}O/^{16}O$ ratios of minerals of possible mantle or lower crustal origin: Earth Planet. Sci. Lett., v. 9, p. 232-239.

Sigvaldason, G. E., and Elisson, G., 1968, Collection and analysis of volcanic gases at Surtsey, Iceland: Geochim. Cosmochim. Acta, v. 32, p. 797-805.

Skinner, B. J., 1966, Thermal expansion in handbook of physical constants: Geol. Soc. America Mem. 97, p. 75-96.

Sobolev, V. S., Bazarova, T. Yu, and Bakumenko, I. T., 1972, Crystallization temperature and gas phase composition of alkaline effusives as indicated by primary melt inclusions in the phenocrysts: Bull. Volcanol., v. 35, no. 2, p. 478-496.

Swanson, D. A., and Fabbi, B. P., 1973, Loss of volatiles during fountaining and flowage of basaltic lava at Kilauea volcano, Hawaii: U. S. Geol. Survey, J. Res., v. 1, p. 642-658.

Taylor, H. P., Jr., 1974, The application of oxygen and hydrogen isotope studies to problems of hydrothermal alteration and ore deposition: Econ. Geol., v. 69, p. 843-883.

Tazieff, H., 1966, New investigations on eruptive gases: Bull. Volcanol., v. 34, p. 421-438.

Tazieff, H., Leguern, F., Carbonnelle, J., and Zettwoog, P., 1972, Etude chimique des fluctuations des gas eruptifs du volcan Erta'Ale: Acad. Sci. Comptes Rendus, ser. D., v. 274, p. 1003-1006.

Walker, D., Kirkpatrick, R. J., Longhi, J., and Hays, I. F., 1975, 12002 revisited in Lunar Science VI: The Lunar Science Inst., Houston, p. 841-843.

Watson, E. B., 1976, Glass inclusions as samples of early magmatic liquid: Determinative method and application to a South Atlantic basalt: Jour. Volcanol. Geotherm. Res., 1, p. 73-84.

Wenner, D. B., and Taylor, H. P., Jr., 1973, Oxygen and hydrogen isotope studies of the serpentinization of ultramafic rocks in oceanic environments and continental ophiolite complexes: Am. Jour. Sci., v. 273, p. 207.